

Article

Not peer-reviewed version

Discovery of Novel 2-Substituted Aniline Pyrimidine Based Derivatives as Potent Mer/c-Met Dual Inhibitors with Improvement Bioavailability

[Jixia Yang](#) , [Daowei Huang](#) ^{*} , Ruojin Wang , Pengxin Fan , Rourou Li , [Donglai Ma](#) ^{*}

Posted Date: 7 May 2025

doi: 10.20944/preprints202505.0411.v1

Keywords: Mer kinase; c-Met kinase; Mer/c-Met dual inhibitor; 2-substituted aniline pyrimidine; Anti-cancer



Preprints.org is a free multidisciplinary platform providing preprint service that is dedicated to making early versions of research outputs permanently available and citable. Preprints posted at Preprints.org appear in Web of Science, Crossref, Google Scholar, Scilit, Europe PMC.

Copyright: This open access article is published under a Creative Commons CC BY 4.0 license, which permit the free download, distribution, and reuse, provided that the author and preprint are cited in any reuse.

Article

Discovery of Novel 2-Substituted Aniline Pyrimidine Based Derivatives as Potent Mer/c-Met Dual Inhibitors with Improvement Bioavailability

Jixia Yang ¹, Daowei Huang ^{2,*}, Ruojin Wang ¹, Pengxin Fan ¹, Rourou Li ¹ and Donglai Ma ^{1,*}

¹ School of Pharmacy, Hebei University of Chinese Medicine, Shijiazhuang 050200, China

² School of Chemical and Pharmaceutical Engineering, Hebei University of Science and Technology, Shijiazhuang 050018, China

* Correspondence: huangdaowei321@163.com (D.W.); mdl_hebei@aliyun.com (D.L.)

Abstract: This study reports the rational design and systematic evaluation of a novel series of 2-substituted aniline pyrimidine derivatives as dual Mer/c-Met inhibitors. Among the synthesized compounds, **17c** demonstrated potent dual kinase inhibition, with IC₅₀ values of 6.4 ± 1.8 nM (Mer) and 26.1 ± 7.7 nM (c-Met). The compound exhibited significant antiproliferative activity across multiple cancer cell lines (HepG2, MDA-MB-231, and HCT116), while showing minimal hERG channel inhibition (IC₅₀ > 40 μM), indicating favorable cardiac safety. Pharmacokinetic profiling revealed high metabolic stability in human liver microsomes (t_{1/2} = 53.1 min) and moderate oral bioavailability (F: 45.3%) with strong plasma protein binding affinity (>95%). Mechanistic studies further demonstrated **17c** dose-dependently suppressed HCT116 cell migration and induced apoptosis. These integrated pharmacological properties position **17c** as a promising therapeutic candidate for dual Mer/c-Met drive malignancies.

Keywords: Mer kinase; c-Met kinase; Mer/c-Met dual inhibitor; 2-substituted aniline pyrimidine; Anti-cancer

1. Introduction

Mer kinase, a key member of TAM (Tyro3-Axl-Mer) receptor tyrosine kinase family [1–3], orchestrates multiple cellular processes critical to immune regulation, apoptosis resistance, and inflammatory signaling. Structurally, Mer is characterized by a conserved intracellular tyrosine kinase domain and extracellular ligand-binding region. Its expression is predominantly localized to immune cell (e.g., macrophages and dendritic cells), where it mediates efferocytosis (apoptotic cell clearance) and suppresses pro-inflammatory cytokine production, thereby maintaining immune tolerance [4]. Mechanistically, Mer activation occurs through Gas6 ligand binding, initiating downstream signaling cascades (e.g., PI3K/AKT, MAPK) that promote cell survival, chemotaxis, and tissue remodeling [4]. Importantly, Mer dysregulation has been pathologically linked to oncogenesis: overexpression in tumor cells enhances survival under chemotherapy (via BCL-2 upregulation), facilitates metastatic dissemination (through EMT activation), and fosters immunosuppressive microenvironments (by polarizing tumor-associated macrophages) [5–8]. These multifaceted roles established Mer as a high-value therapeutic target for precision oncology strategies targeting both tumor-intrinsic and immune-evasion mechanisms.

Current Mer kinase inhibitors are structurally categorized into two major chemotypes: aminopyrimidine-pyrazole (pyrrole) and aminopyrimidine derivatives (Figure 1). The first-generation inhibitor UNC569 [9,10], a pyrazole-based compound, selectively inhibits Mer kinase (IC₅₀ = 1.2 nM) and suppresses downstream ERK/AKT signaling. However, its clinical translation is hindered by rapid metabolism (human microsomal t_{1/2} < 15 min) and low oral bioavailability (F < 10%) [11]. Structural optimization of UNC569 yielded second-generation analogs. UNC2025: enhanced

metabolic stability ($t_{1/2}$ = 68 min in human hepatocytes) with maintained Mer potency (IC_{50} = 1.8 nM) [12,13]. MRX2843: dual Mer/Flt3 inhibitor (Mer IC_{50} = 1.2 nM) showing improved CNS penetration (brain/plasma ratio = 0.4) [11], currently in phase II trials for relapsed/refractory acute lymphoblastic leukemia (NCT04872478) [14]. Notably, the aminopyrimidine-class inhibitor UNC2250 demonstrates exceptional Mer targeting (IC_{50} = 1.7 nM) and unique activity against Mer-EGFR fusion protein [15,16]. In xenograft models, UNC2250 induced tumor regression (~60% volume reduction vs. control) by dual blockade of Mer-mediated survival signaling and EGFR-driven proliferation [16].

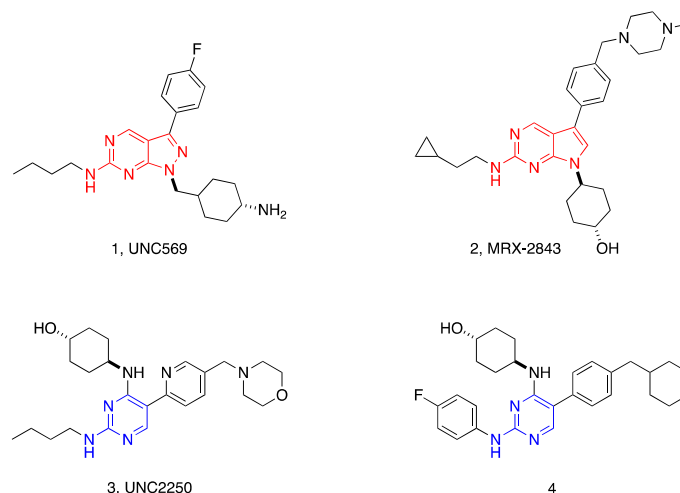


Figure 1. The representative Mer inhibitors.

The c-Met kinase, also known as the hepatocyte growth factor receptor (HGFR) [17,18], is a transmembrane receptor tyrosine kinase that plays a pivotal role in regulating critical cellular processes, including proliferation, survival, migration, and angiogenesis [19,20]. Activation of c-Met occurs through binding to its specific ligand HGF, which triggers receptor dimerization and autophosphorylation. This activation initiates downstream signaling cascades, such as the MAPK, PI3K/AKT, and STAT pathways. Aberrant c-Met signaling, caused by overexpression, mutations, or gene amplification, is strongly associated with tumorigenesis, promoting cancer progression, metastasis, and therapy resistance. Given its oncogenic significance, c-Met has become a promising therapeutic target. Current clinical investigations are actively exploring both small-molecule inhibitors and monoclonal antibodies targeting c-Met for the treatment of diverse malignancies.

Multiple c-Met inhibitors have entered clinical practice or are under clinical investigation (Figure 2). Notably, crizotinib, approved by the FDA in 2011, is primarily used for ALK-positive metastatic non-small cell lung cancer (NSCLC) but also exhibits c-Met inhibitory activity as part of its multi-target mechanism [21,22]. Cabozantinib, another tyrosine inhibitor targeting c-Met, VEGFR, Mer, and Kit, has been approved for multiple indications: metastatic medullary thyroid cancer, second-line treatment of advanced renal cell carcinoma post-antiangiogenic therapy, and first-line therapy for advanced renal cell carcinoma [23,24]. Additionally, savolitinib—a highly selective c-Met inhibitor—is currently in Phase III clinical trials for papillary renal cell carcinoma and other c-Met-driven malignancies [25]. Capmatinib, a selective c-Met inhibitor, received FDA approval specifically for metastatic NSCLC with MET exon 14 skipping mutations [26,27].

Mer and c-Met, both members of the receptor tyrosine kinase family, exhibit structurally homologous extracellular domains and share overlapping downstream signaling pathways. Notably, their functional convergence in regulating tumor proliferation, metastasis, and immune evasion establishes a compelling rationale for dual targeting of Mer and c-Met kinases. To date, cabozantinib and its derivatives remain the only clinical available agent with demonstrated inhibitory activity against both targets. However, cabozantinib's clinical utility is predominantly attributed to its potent

inhibition of c-Met and VEGFR-2, while the structural determinants governing its Mer kinase inhibitory activity remains poorly characterized. Furthermore, the emergence of cabozantinib resistance underscores the critical need to develop novel Mer/c-Met dual inhibitors with distinct chemical scaffolds. Importantly, the structure-activity relationship (SAR) of Mer/c-Met dual inhibitors remains underexplored, systematic exploration of these aspects through rational drug design is therefore essential to advance the development of next-generation dual-targeting agents.

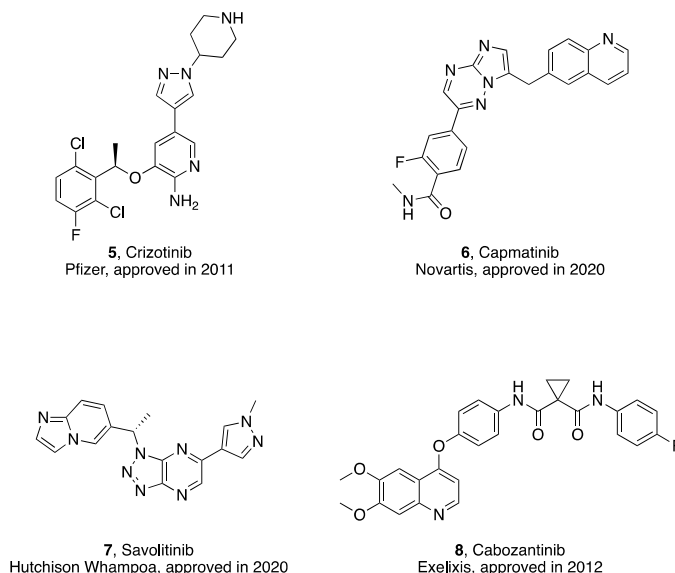


Figure 2. The representative c-Met inhibitors.

Previous study identified compound **18c** as a dual Mer/c-Met dual inhibitor with potent dual-target inhibitory activity [28]. However, pharmacokinetic analysis revealed low oral bioavailability (F: 2.84%), promoting structural optimization. To elucidate key interaction for dual-target inhibition, we analyzed the binding modes of cabozantinib with Mer (PDB: 4M3Q) and c-Met (PDB: 3LQ8). Molecular docking showed that in Mer kinase, cabozantinib's amide group forms hydrogen bonds with the hinge region (Pro672 and Met674), while the quinoline moiety occupies a hydrophobic cavity without direct hydrogen bonding (Figure 3). In c-Met kinase, both the quinoline core and the amide group participate in hydrogen bonding with residues in the ATP-binding pocket (Figure 4). Based on these observations and the binding mode of **18c** [28], we propose modifying the 2-position of the pyrimidine ring to introduce hydrophilic groups. This strategy aims to enhance solubility and bioavailability while preserving dual-target activity.

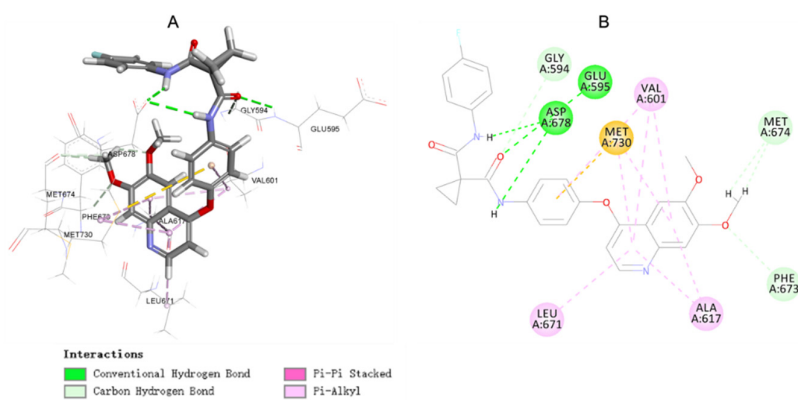


Figure 3. The docking mode of cabozantinib with Mer kinase (PDB: 4M3Q), A) 3D binding mode; B) 2D binding mode.

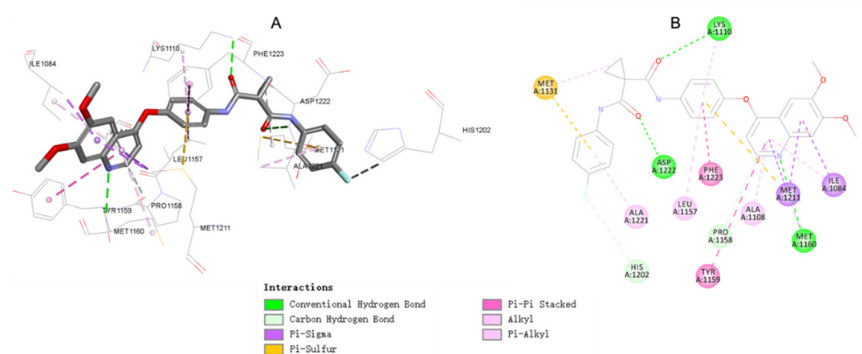


Figure 4. The docking mode of cabozantinib with c-Met kinase (PDB: 3LQ8), A) 3D binding mode; B) 2D binding mode.

Building upon our previous work (Figure 5), we designed and synthesized a series of 2-substituted aniline pyrimidine derivatives, with subsequent evaluation of their biological activities. Among these, compound **17c** emerged as a lead candidate due to its superior metabolic stability in human liver microsomes and potent antiproliferative activities against three cancer cell lines (HepG2, MDA-MB-231, and HCT116). **17c** also revealed favorable Pharmacokinetic properties, plasma protein binding, and favorable safety profile in hERG assays. Mechanistic studies further showed **17c** induced dose-dependent apoptosis in HCT116 cells and effectively inhibited HCT116 cell migration. These results position **17c** as a promising dual Mer/c-Met inhibitor warranting further development.

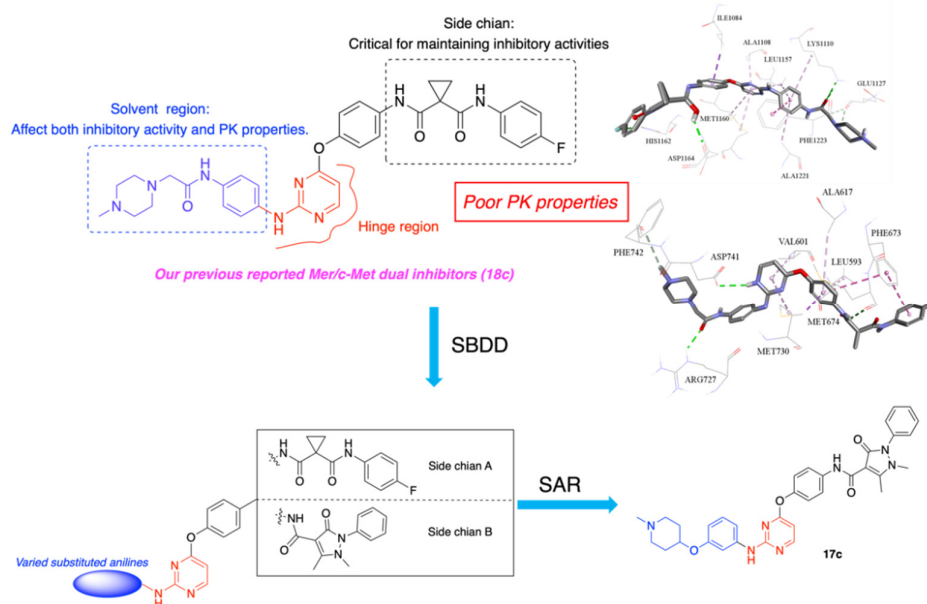


Figure 5. Design strategy of target compounds.

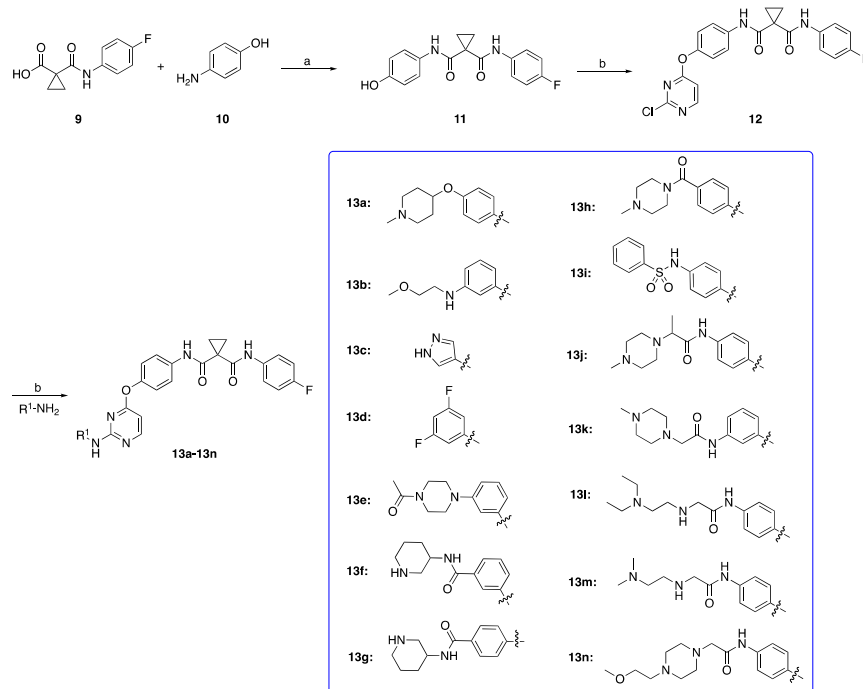
2. Results and Discussion

2.1. Chemistry

The synthesis of target compounds and key intermediates are described in Schemes 1 and 2, respectively. The structures of compounds were confirmed by $^1\text{H-NMR}$, $^{13}\text{C-NMR}$ and HRMS spectroscopy.

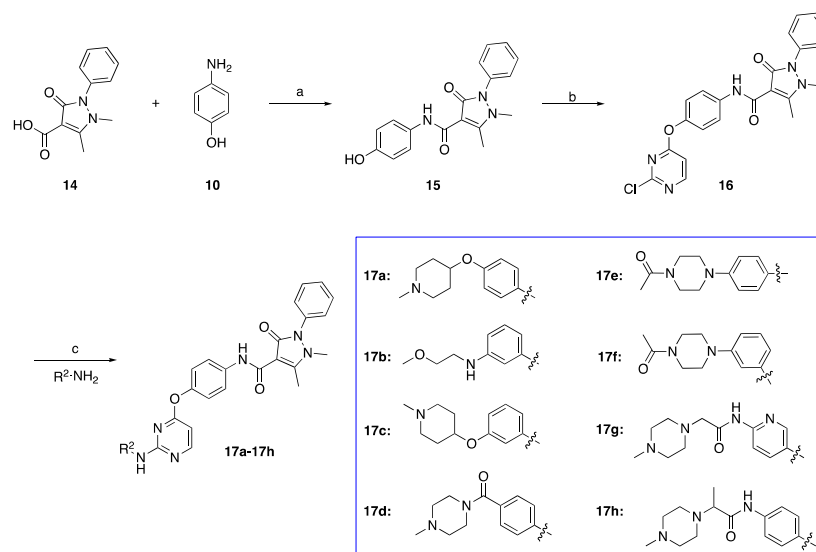
As depicted In scheme 1, a condensation reaction was employed where 1-((4-fluorophenyl)carbamoyl)cyclopropane-1-carboxylic acid (**9**) was combined with readily accessible 4-aminophenol (**10**) at ambient temperature, yielding the intermediate *N*-(4-fluorophenyl)-*N*-(4-

hydroxyphenyl)cyclopropane-1,1-dicarboxamide (**11**) [29]. Subsequently, the intermediate *N*-(4-((2-chloropyrimidin-4-yl)oxy)phenyl)-*N*-(4-fluorophenyl)cyclopropane-1,1-dicarboxamide (**12**) was produced via an S_N2 reaction between intermediate **11** with 2,4-dichloropyrimidine [30]. Finally, the desired compounds **13a–13h** were obtained by reacting intermediate **12** with various substituted anilines, which were either commercial available or prepared in our prior research [31].



Scheme 1. Reagents and conditions: (a) EDC·HCl/DMF, r.t., 6 h; (b) K_2CO_3 /DMF, 80 °C, 6 h; (c) PTSA/DMF, 90 °C, 4 h.

In Scheme 2, the preparation of the crucial intermediate *N*-(4-hydroxyphenyl)-1,5-dimethyl-3-oxo-2-phenyl-2,3-dihydro-1*H*-pyrazole-4-carboxamide (**15**) commenced with a condensation process involving 1,5-dimethyl-3-oxo-2-phenyl-2,3-dihydro-1*H*-pyrazole-4-carboxylic acid (**14**) and with 4-aminophenol (**10**) [32]. The intermediate **15** was then reacted with 2,4-dichloropyrimidine, yielding in the forming of the pivotal intermediate *N*-(4-((2-chloropyrimidin-4-yl)oxy)phenyl)-1,5-dimethyl-3-oxo-2-phenyl-2,3-dihydro-1*H*-pyrazole-4-carboxamide (**16**). The target compounds **17a–17h** were subsequently obtained by carrying out a nucleophilic substituted reaction between intermediate **16** and various substituted anilines.



Scheme 2. Reagents and conditions: (a) HBTU/TEA/DMF, r.t., 8 h; (b) K_2CO_3 /DMF, 80 °C, 4.5 h; (c) PTSA/DMF, 90 °C, 4.0 h.

2.2. Kinase Inhibitory Activities

All the target compounds (supplementary material, S1) were initially screened for their inhibitory activities on Mer and c-Met kinases compared to the lead compound (**18c**), and the results were depicted in Table 1 and Table 2. The corresponding curves were showed in Supplementary S3 and S4.

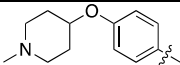
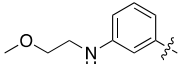
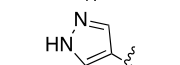
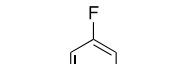
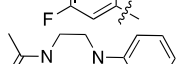
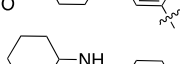
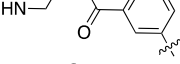
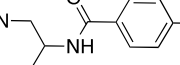
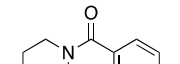
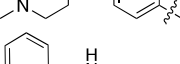
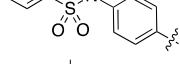
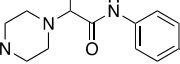
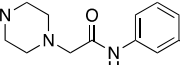
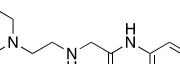
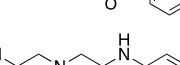
As summarized in Table 1, the substituents (R^1) at the terminal pyrimidine amine group significantly modulate inhibitory potency against Mer and c-Met kinases. Compounds **13b**, **13j**, **13k**, **13m**, and **13n** exhibited moderate to potent dual inhibitory, with Mer IC_{50} values ranging from $13.1 \pm 2.1 \sim 37.3 \pm 10.6$ nM and c-Met IC_{50} values of $25.9 \pm 7.7 \sim 48.6 \pm 11.2$ nM, compared to the lead compound **18c** (Mer IC_{50} : 18.5 ± 2.3 nM, c-Met IC_{50} : 33.6 ± 4.3 nM). Strikingly, compound **13e** demonstrated the highest dual potency, achieving IC_{50} values of 7.5 ± 1.6 nM (Mer) and 7.5 ± 1.1 nM (c-Met), representing a 2.5-fold and 4.5-fold improvement over **18c**, respectively. In contrast, compounds **13c** and **13h** showed reduced Mer inhibitory activity while maintaining c-Met inhibitory activity comparable to **18c**. Conversely, compounds **13d**, **13i**, and **13l** exhibited significantly reduced inhibitory activities against both Mer and c-Met kinase.

A novel series of pyrimidine derivatives were designed to optimize dual Mer/c-Met inhibition. As shown in Table 2, the Mer kinase inhibitory activities varied significantly across the series. Compounds **17d**, **17e**, and **17g** exhibited reduced inhibitory potency, with Mer IC_{50} values of 84.1 ± 13.9 , 69.8 ± 12.5 , and >1000 nM, respectively. In contrast, compounds **17a**, **17b**, and **17h** retained activity comparable to the lead compound, featuring IC_{50} values of 26.2 ± 7.1 , 12.1 ± 1.3 , and 11.9 ± 1.7 nM. Notably, compounds **17c** and **17f** showcased superior inhibition, achieving Mer IC_{50} values of 6.4 ± 1.8 nM and 5.5 ± 0.8 nM.

For c-Met kinase inhibition, compounds **17c**, **17f**, and **17h**, exhibited comparable IC_{50} values ranging from 25.0 ± 3.5 to 45.0 ± 6.8 nM. However, the potency of **17a**, **17b**, **17d**, **17e**, and **17g** decreased (IC_{50} values from 100.7 ± 18.5 nM to 235.6 ± 25.6 nM), indicating that specific structural optimization at the pyrimidine scaffold detrimentally impact c-Met binding.

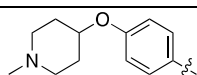
The findings converge to demonstrate that the designed compounds exhibit robust inhibitory effects on both Mer and c-Met targets. A general structure-activity relationship can be visualized in Figure 6 and Figure 7.

Table 1. Inhibitory activities of compound **13a–13n** against Mer and c-Met kinase.

Compd.	R ¹	IC ₅₀ (nM) ¹	
		Mer	c-Met
13a		21.7 ± 5.8	63.3 ± 9.1
13b		24.3 ± 5.7	25.9 ± 7.7
13c		110.1 ± 15.7	48.9 ± 6.4
13d		640.2 ± 82.2	728.1 ± 131.4
13e		7.5 ± 1.6	7.5 ± 1.1
13f		>1000	>1000
13g		>1000	>1000
13h		72.0 ± 8.9	41.6 ± 8.5
13i		>1000	946.4 ± 15.1
13j		30.2 ± 5.1	27.8 ± 3.8
13k		25.6 ± 3.8	39.4 ± 5.1
13l		95.3 ± 20.1	88.6 ± 13.9
13m		13.1 ± 2.1	48.6 ± 11.2
13n		37.3 ± 10.6	35.4 ± 10.0
18c		18.5 ± 2.3	33.6 ± 4.3

¹Data are means from three independent experiments.

Table 2. Inhibitory activities of compound **17a–17h** against Mer and c-Met kinase.

Compd.	R ²	IC ₅₀ (nM) ¹	
		Mer	c-Met
17a		26.2 ± 7.1	233.4 ± 25.4

17b		12.1 ± 1.3	100.7 ± 18.5
17c		6.4 ± 1.8	26.1 ± 7.7
17d		84.1 ± 13.9	137.1 ± 34.3
17e		69.8 ± 12.5	235.6 ± 25.6
17f		5.5 ± 0.8	25 ± 3.5
17g		>1000	139.7 ± 18.9
17h		11.9 ± 1.7	45.0 ± 6.8
18c		18.5 ± 2.3	33.6 ± 4.3

¹Data are means from three independent experiments.

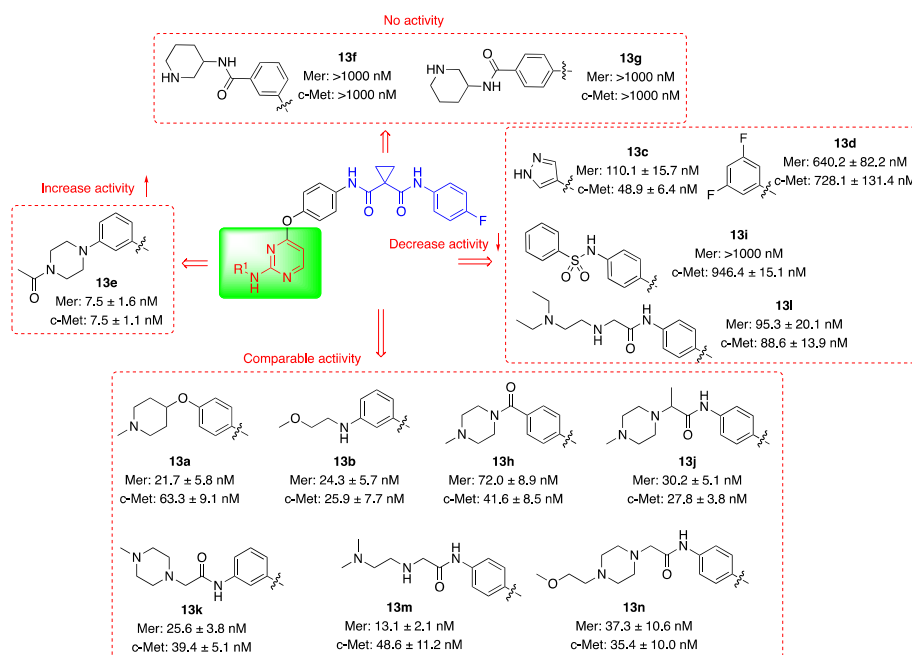


Figure 6. SAR study of the designed compounds with side chain A.

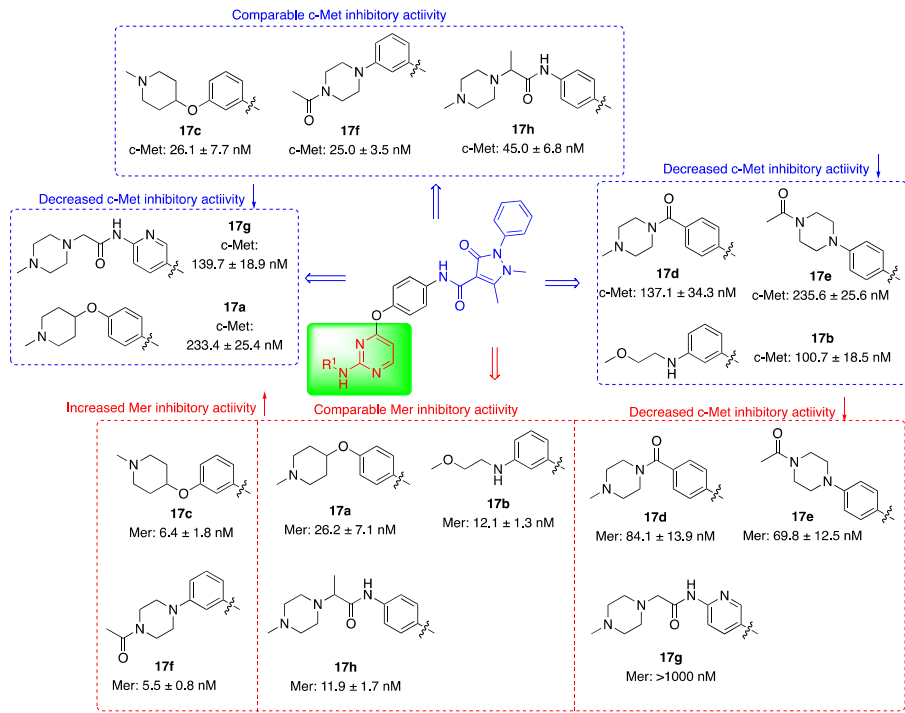


Figure 7. SAR study of the designed compounds with side chain B.

2.3. In Vitro Liver Microsomal Stability

Metabolic stability is a critical determinant of drug-like properties. To prioritize compounds for further development, we evaluate the human liver microsomal stability of selected candidates demonstrating potent dual Mer/c-Met dual inhibition in vitro. As shown in Table 3, compounds **13b**, **13e**, **13j**, **13k**, **13m**, **13n**, **17c**, and **17f** were subjected to microsome assays to determine their half-life and intrinsic clearance. Compound **17c** demonstrated superior metabolic stability, with an extended $t_{1/2}$ of 147.0 min and low CL_{int} of 0.026 mL/min/mg, whereas **17f** exhibited a shorter $t_{1/2}$ of 51.0 min and higher CL_{int} of 0.068 mL/min/mg. Notably, all other compounds showed rapid hepatic clearance ($t_{1/2}$ < 40 min, CL_{int} > 0.068 mL/min/mg), suggesting limited metabolic resistance. The results highlight **17c** as the most metabolically stable candidate within this series.

Table 3. Microsome stability study of compound **13b**, **13e**, **13j**, **13k**, **13m**, **13n**, **17c**, and **17f**.

Cpd.	HUMAN	
	T _{1/2} (min)	CL (mL/min/mg)
13b	38.3	0.0905
13e	30.4	0.1142
13j	11.9	0.2912
13k	8.6	0.4046
13m	27.9	0.1521
13n	38.4	0.1243
17c	147.0	0.0236
17f	51.0	0.0680

Testosterone	32.1	0.11
--------------	------	------

2.4. Antiproliferation Assay In Vitro

Compound **17c** was further evaluated for its antiproliferative activity against three cancer cell lines with high Mer and c-Met expression (HCT116 colon cancer, CAKI-1 renal cancer, and PC-3 prostate cancer) using CCK-8 assay [5,33–35]. As summarized in Table 4, **17c** demonstrated superior antiproliferative activity compared to cabozantinib across all tested cell lines. Notably, **17c** exhibited marked most potency with HCT116 cells, with an IC₅₀ value of 0.46 ± 0.06 μmol/L—a 17.1-fold improvement over cabozantinib. In CAKI-1 cells, **17c** showed an IC₅₀ of 2.31 ± 0.67 μmol/L, representing a 2.0-fold enhancement compared to cabozantinib. Similarly, against PC-3 cells, **17c** achieved an IC₅₀ of 3.79 ± 1.09 μmol/L, which is 4.1 times more effective than cabozantinib. These results collectively establish compound **17c** as a potent dual Mer/c-Met inhibitor with significant therapeutic potential. The dose-response curves are provided in Supplementary S5.

Table 4. Cytotoxic activities of compound **17c** on cancer cell lines in vitro.

Cpds	IC ₅₀ (μM) ¹ of 3 cell lines		
	HepG2	MDA-MB0231	HCT116
17c	0.46 ± 0.06	2.31 ± 0.67	3.79 ± 1.09
Cabozantinib	7.87 ± 2.11	4.62 ± 0.54	15.57 ± 4.39

¹Data are means from three independent experiments.

2.5. Molecular Docking Study of Compound 17c

Molecular docking was conducted to validate the binding mode of compound **17c** with Mer kinase (PDB: 4M3Q) and c-Met (PDB: 3LQ8) kinases. As illustrated in Figure 8, the docking pose of **17c** in Mer kinase revealed three critical interactions: (1) the aminopyrimidine moiety acts as hydrogen bond acceptor with Leu593; (2) the amide side chain forms a hydrogen bond with Lys619; (3) the benzene ring of side chain engages in a π-π stacking interaction. For c-Met kinase (Figure 9), **17c** exhibited a similar binding mode: (1) the aminopyrimidine core forms a hydrogen bond with Met1160; (2) the amide group forms hydrogen bonds with Lys1110 and Phe1223; (3) the pyrimidine group participates in π-π interaction. These results confirm that the 2-substitutedaniline pyrimidine group effectively occupies the ATP-binding pockets of both kinases through conserved hydrogen bonding and hydrophobic interactions. The structural coherence between predicted binding modes and enzymes inhibitory data strongly supports the rational design strategy, validating the scaffold's potential for dual Mer/c-Met inhibition.

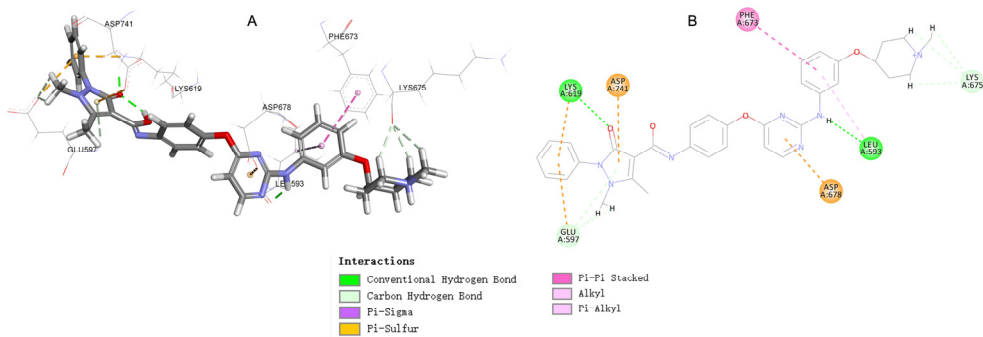


Figure 8. The docking mode of **17c** with Mer kinase (PDB: 4M3Q). A) 3D binding mode; B) 2D binding mode.

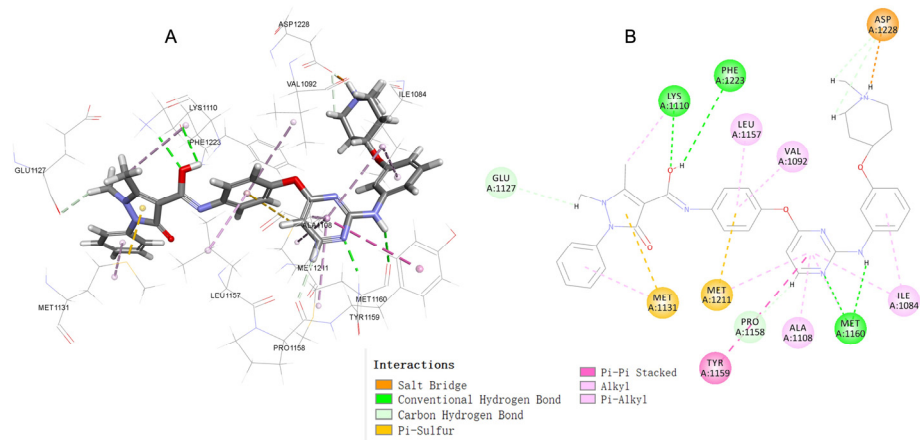


Figure 9. The docking mode of **17c** with c-Met kinase (PDB: 3LQ8), A) 3D binding mode; B) 2D binding mode.

2.6. Western Blot Assay

The inhibitory effects of compound **17c** on Mer and c-Met kinase phosphorylation were assessed using Western blot analysis. As shown in Figure 10, increasing concentrations of **17c** resulted in a reduction in the phosphorylation levels of both Mer and c-Met kinases. At a concentration of 2.5 μM , **17c** significantly inhibited the phosphorylation of these kinases compared to the positive control, demonstrating its potential to effectively block Mer and c-Met kinase activation.

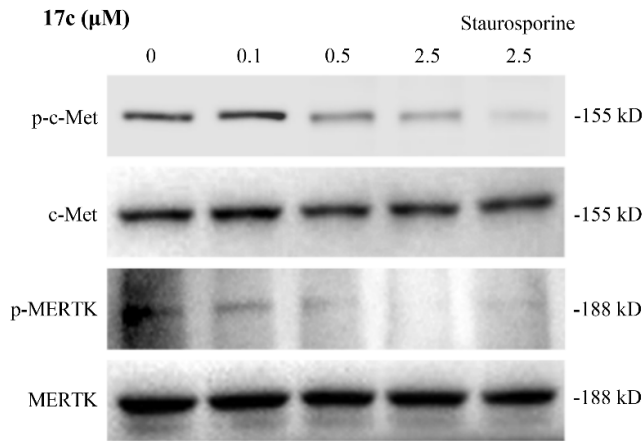


Figure 10. Western blot analysis was applied to analyze the expression and phosphorylation of c-Met and MERTK in HCT116 cells with staurosporine or increasing doses of compound **17c**. All experiments were performed at least three times.

2.7. The hERG Test

To evaluate the potential cardiotoxicity risk associated with compound **17c**, we assessed its inhibitory activity against the hERG potassium channel, a key determinant of cardiac safety. As summarized in Table 5, **17c** demonstrated negligible hERG inhibition ($\text{IC}_{50} > 40 \mu\text{M}$), indicating a low risk of hERG activity was observed despite its potent dual inhibition of Mer and c-Met kinases.

Table 5. Activity on hERG potassium currents of compound **17c**.

Cpd.	IC_{50} (μM)
17c	>40

Cisapride	0.04
-----------	------

2.8. Apoptosis Assay

To evaluate the apoptosis-inducing capability of compound **17c**, the HCT116 colon cancer cell line was treated with varying concentrations of the compound. Apoptosis was evaluated using the TUNEL assay. DAPI staining (blue) was served as the positive control, while apoptotic cells were identified by TUNEL staining (green) after 48 h incubation with compound **17c**, as shown in Figure 11. The quantity of apoptotic cells was measured at different concentrations of **17c**, resulting in an ED₅₀ value of 2.036 μ M. These results demonstrate that compound **17c** efficiently triggers apoptosis in HCT116 cells, thereby emphasizing its potential as a highly promising candidate for additional research and development.

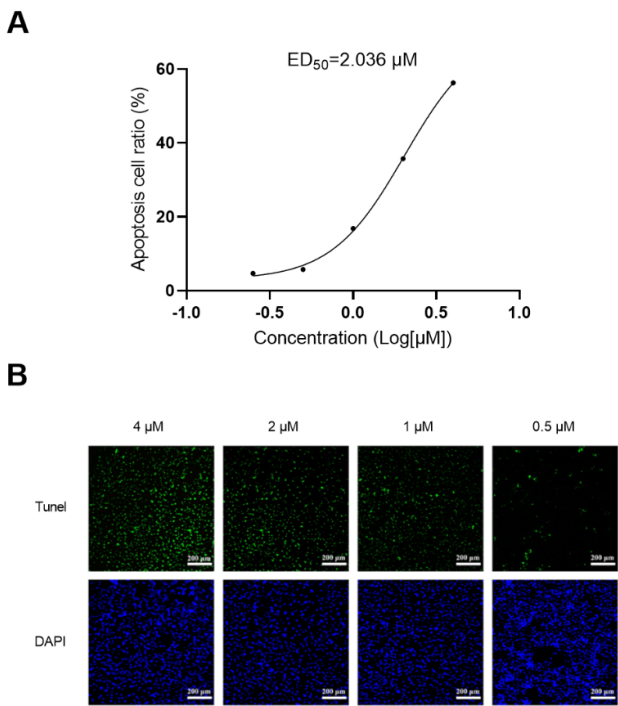


Figure 11. Compound **17c** induced cell apoptosis in HCT116 cancer cell. (A) Quantitative analysis of TUNEL staining. (B) Representative TUNEL and DAPI-stained images. Magnification, x100. HCT116 cells grown on cover slip, treated with various indicated dose of **17c** for 48 h, and stained for TUNEL (green). The number of TUNEL-positive cells were counted from 5 non-overlap random fields per group. DAPI (blue). Data are representative of three independent experiments.

2.9. Transwell Assay

The Transwell migration assay shown in Figure 12 was performed to evaluate the effect of compound **17c** on the migration of HCT116 cells. A decrease in the number of cells migrating through the membrane was observed with increasing concentration of **17c**. These results suggest that compound **17c** effectively inhibits the migration capacity of HCT116 colon cancer cells in a concentration-dependent manner.

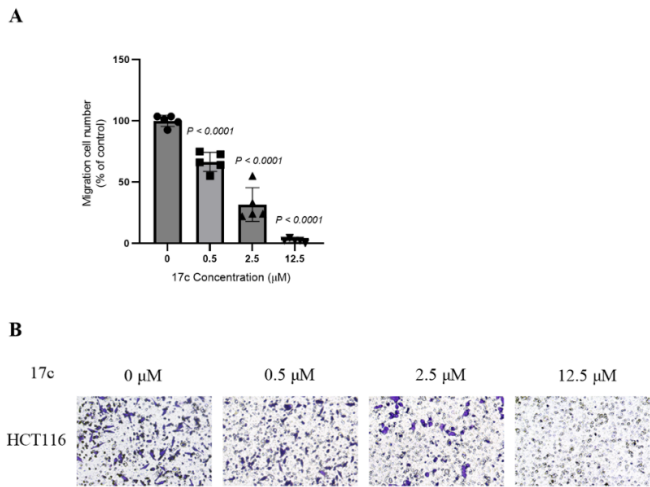


Figure 12. Compound **17c** inhibited cell migration in HCT116 cancer cell. (A) Representative images of transwell assay of HCT116 cells treated with compound **17c** for 24 h. (B) Quantification of transwell assays.

2.10. Plasma Protein Binding Affinity

The plasma protein binding (PPB) profile of compound **17c** was assessed via equilibrium dialysis, with warfarin served as a positive control. As shown in Table 6, **17c** exhibited high species-independent protein binding, with unbound fractions of 1.58% in human plasma and 1.78% in mouse plasma, corresponding to PPB values of 98.4% and 98.2%, respectively. Combined with its extended half-life and low clearance, the high PPB of **17c** may contributed to sustained target engagement.

Table 6. Stability recovery of compound **17c** and positive control in plasma.

Cpd.	Con. (μM)	Species	Mean Fu	Mean Fb	Stability (%)
17c	1	Human	0.0158	98.4%	99.3%
17c	1	Rat	0.0178	98.2%	102.2%
Warfarin	1	Human	0.00877	99.1%	99.8%
Warfarin	1	Rat	0.0102	99.0%	98.2%

Fu=Area ratio of compound in buffer/Area ratio of compound in plasma. Fb=100×(1–Fu).

2.11. Pharmacokinetic Properties

The Pharmacokinetic (PK) profiles of compound **17c** were evaluated in Sprague-Dawley (SD) rats following single-dose administration via oral (PO) and intravenous (iv) route. As summarized in Table 7, oral administration of **17c** achieved a peak plasma concentration (C_{max}) of 740 ng/mL, at T_{max} = 4.0 h, with a half-time (T_{1/2}) of 3.46 h and a mean residence time (MRT_{inf}) of 6.52 h. Compared to lead compound **18c**, compound **17c** demonstrated significantly improved PK properties, including prolonged oral half-time, reduced clearance, an extended mean residence time, and enhanced oral bioavailability (45.3%). These data indicate that **17c** exhibits favorable PK properties, with sustained drug exposure and optimized absorption characteristics.

Table 7. Pharmacokinetic parameters of compound **17c**.

Adm.	Dose (mg/Kg)	AUC _{last} (h*ng/mL)	T _{1/2} (h)	T _{max} (h)	C _{max} (ng/mL)	CL _{obs} (mL/min/kg)	MRTINF _{obs} (h)	F (%)
p.o.	10	4626	3.46	4.00	740	–	6.52	45.3

i.v.	2	2154	3.33	–	–	16.4	3.23
------	---	------	------	---	---	------	------

3. Materials and Methods

3.1. Chemical Part

All reagents were obtained from Titan Chemical Co., Ltd., and solvents were obtained from Shijiazhuang Kehai Huabo Instruments Co., Ltd., which were used without further purification unless otherwise indicated. All the Reactions were monitored by thin layer chromatography (TLC) using silica GF254 Plates. High Resolution Mass spectra (HRMS) were performed in electrospray ionization (ESI) mode on a Water Q-ToF mass spectrometer. Proton (¹H) and carbon (¹³C) nuclear magnetic resonance (NMR) spectra were generated in DMSO-d₆ on Bruker AM-400 and AM500 spectrometers (Bruker Bioscience, USA), with tetramethylsilane (TMS) as the internal reference, and chemical shift values were reported in ppm. The multiplicity of the signals is denoted as follows: s (singlet); d (doublet), t (triplet), q (quadruplet), qui (quintuplet), m (multiplet), dd (doublet of doublets), and dt (doublet of triplets). Coupling constants (*J*) are given in hertz (Hz). Flash chromatography was performed using silica gel (200-300 mesh) as the stationary phase, with a mobile phase consisting of a mixture of methanol (MeOH), ethyl acetate (EA), and petroleum ether (PE). The purity of all synthesized compounds was confirmed to be >95% by high-performance liquid chromatography (HPLC) using a Waters HPLC system equipped with a UV/visible detector, monitored at 254 nm. HPLC analysis was carried out on a 5 μm, 4.6 × 250 mm Hypersil ODS2 column, with a mobile phase consisting of a 3:7 (v/v) mixture of potassium dihydrogen phosphate solution and methanol, at a flow rate of 1.0 mL/min and an injection volume of 10 μL. All chemicals were of analytical grade and used without further purification.

3.1.1. Preparation of N-(4-Fluorophenyl)-N-(4-hydroxyphenyl)cyclopropane-1,1-dicarboxamide (Intermediate 11)

To a solution of 1-((4-fluorophenyl)carbamoyl)cyclopropane-1-carboxylic acid (2.02 g, 9.00 mmol) and 4-aminophenol (1.18 g, 10.8 mmol) in DMF (5 mL), EDC·HCl (2.07 g, 10.80 mmol) was added. The reaction solution was stirred at room temperature for 6 h and monitored by TLC. Ice water (125 mL) was added, and the precipitate was filtered off, washed, and dried in a vacuum to yield Intermediate **11** as a white solid (2.28 g, 80.6%), which can be used for the next step without any purification.

3.1.2. Preparation of N-(4-((2-Chloropyrimidin-4-yl)oxy)phenyl)-N-(4-fluorophenyl)cyclopropane-1,1-dicarboxamide (Intermediate 12)

To a solution of intermediate **11** (2.01 g, 6.37 mmol) and 2,4-dichloropyrimidine (1.04 g, 7.01 mmol) in DMF (15 mL), K₂CO₃ (0.97 g, 7.01 mmol) was added under N₂ atmosphere. The reaction solution was stirred at 80 °C for 6 h and monitored by TLC. The reaction mixture was poured into ice water (100 mL), and the precipitate was filtered off, washed, and dried in a vacuum to obtain the crude product, which was purified by silica gel chromatography using a mixture of (DCM: MeOH = 100:1~40:1) to afford the intermediate **12** as a white solid (2.34 g, 75.70 %).

3.1.3. General Procedure for Preparation of Target Compounds 13a–13n

To a mixture of the intermediate **12** (1.2 mmol), substituted aniline (1.0 mmol), and DMF (8 mL), p-toluenesulfonic acid (PTSA, 4.0 mmol) was added. The mixture was stirred at 90 °C for 4 h under N₂ atmosphere. The reaction solution was cooled to room temperature, then poured into ice water (100 mL), and the precipitate was filtered off, washed, and dried in a vacuum to obtain the crude product, which was purified by silica gel chromatography using a mixture of (DCM: MeOH = 100:1-40:1) to afford the product **13a–13n**.

N-(4-fluorophenyl)-N-(4-((2-((4-((1-methylpiperidin-4-yl)oxy)phenyl)amino)pyrimidin-4-yl)oxy)phenyl)cyclopropane-1,1-dicarboxamide (compound **13a**): White solid, yield: 23.27%. ¹H NMR (500 MHz, DMSO-*d*₆) δ 10.18 (s, 1H), 10.11 (s, 1H), 9.41 (s, 1H), 8.30 (d, *J* = 5.6 Hz, 1H), 7.70 (d, *J* = 8.9 Hz, 2H), 7.66 (dd, *J* = 9.1, 5.1 Hz, 2H), 7.43 (d, *J* = 7.5 Hz, 2H), 7.19–7.14 (m, 4H), 6.80 (d, *J* = 8.7 Hz, 2H), 6.35 (d, *J* = 5.6 Hz, 1H), 4.44 (s, 1H), 3.16–2.87 (m, 4H), 2.63 (s, 3H), 2.10–2.01 (m, 2H), 1.85 (s, 2H), 1.51 (d, *J* = 4.6 Hz, 4H). ¹³C NMR (126 MHz, DMSO-*d*₆) δ 170.06, 168.73 (d, *J* = 4.3 Hz, 1C), 160.19, 159.70, 157.79, 151.65, 148.59, 136.63, 135.66, 134.42, 122.86 (d, *J* = 7.7 Hz, 1C), 122.43 (d, *J* = 10.0 Hz, 1C), 120.91, 116.61, 115.62, 115.44, 98.07, 78.48, 50.54, 43.37, 32.01, 28.45, 15.91. HRMS: *m/z* C₃₃H₃₃FN₆O₄ [M+H]⁺ 597.2547, Found 597.2628. Purity: > 95% (HPLC).

N-(4-fluorophenyl)-N-(4-((2-((3-((2-methoxyethyl)amino)phenyl)amino)pyrimidin-4-yl)oxy)phenyl)cyclopropane-1,1-dicarboxamide (compound **13b**): White solid, yield: 20.08%. ¹H NMR (500 MHz, DMSO-*d*₆) δ 10.15 (s, 1H), 10.08 (s, 1H), 9.27 (s, 1H), 8.31 (d, *J* = 5.6 Hz, 1H), 7.71 (d, *J* = 9.0 Hz, 2H), 7.66 (dd, *J* = 9.0, 5.1 Hz, 2H), 7.21–7.14 (m, 4H), 6.86–6.79 (m, 3H), 6.34 (d, *J* = 5.6 Hz, 1H), 6.16 (d, *J* = 7.3 Hz, 1H), 5.21 (s, 1H), 3.44 (t, *J* = 5.9 Hz, 2H), 3.26 (s, 3H), 3.06 (t, *J* = 5.8 Hz, 2H), 1.49 (s, 4H). ¹³C NMR (126 MHz, DMSO-*d*₆) δ 169.90, 168.67, 160.37, 160.22, 159.70, 157.79, 148.56, 141.27, 136.65, 135.67 (d, *J* = 2.0 Hz, 1C), 129.15, 122.82 (d, *J* = 7.7 Hz, 1C), 122.27, 115.61, 115.43, 107.93, 106.71, 103.23, 98.27, 70.93, 58.45, 42.93, 31.95, 15.86. HRMS: *m/z* C₃₀H₂₉FN₆O₄ [M+H]⁺ 557.2234, Found 557.2312. Purity: > 95% (HPLC).

N-(4-((2-((1H-pyrazol-4-yl)amino)pyrimidin-4-yl)oxy)phenyl)-N-(4-fluorophenyl)cyclopropane-1,1-dicarboxamide (compound **13c**): White solid, yield: 31.52%. ¹H NMR (500 MHz, DMSO-*d*₆) δ 12.31 (s, 1H), 10.17 (s, 1H), 10.08 (s, 1H), 9.65–9.18 (m, 1H), 8.29 (s, 1H), 7.72 (s, 2H), 7.65 (dd, *J* = 8.7, 5.0 Hz, 3H), 7.30–7.11 (m, 5H), 6.30 (d, *J* = 5.5 Hz, 1H), 1.50 (s, 4H). ¹³C NMR (126 MHz, DMSO-*d*₆) δ 170.46, 168.68 (d, *J* = 11.7 Hz, 1C), 160.42, 159.84, 159.71, 157.80, 148.56, 136.67, 135.63, 130.12, 122.87 (d, *J* = 6.0 Hz, 1C), 122.40, 122.13, 115.62, 115.44, 98.04, 31.89, 15.97. HRMS: *m/z* C₂₄H₂₀FN₇O₃ [M+H]⁺ 474.1612, Found 474.1686. Purity: > 95% (HPLC).

N-(4-((2-((3,5-difluorophenyl)amino)pyrimidin-4-yl)oxy)phenyl)-N-(4-fluorophenyl)cyclopropane-1,1-dicarboxamide (compound **13d**): White solid, yield: 19.40%. ¹H NMR (400 MHz, DMSO-*d*₆) δ 10.23 (s, 1H), 10.07 (s, 1H), 10.01 (s, 1H), 8.47 (d, *J* = 5.6 Hz, 1H), 7.78 (d, *J* = 8.8 Hz, 2H), 7.69 (dd, *J* = 8.7, 5.1 Hz, 2H), 7.34 (d, *J* = 9.4 Hz, 2H), 7.28–7.17 (m, 4H), 6.67 (t, *J* = 9.1 Hz, 1H), 6.59 (d, *J* = 5.6 Hz, 1H), 1.53 (d, *J* = 4.1 Hz, 4H). ¹³C NMR (101 MHz, DMSO-*d*₆) δ 170.09, 168.56, 160.40, 159.61, 157.59, 148.25, 143.31, 137.04, 135.59 (d, *J* = 2.6 Hz, 1C), 122.93 (d, *J* = 7.8 Hz, 1C), 122.29, 122.05, 115.62, 115.40, 101.74, 101.44, 99.97, 31.88, 15.93. HRMS: *m/z* C₂₇H₂₀F₃N₅O₃ [M+H]⁺ 520.1518, Found 520.1594. Purity: > 95% (HPLC).

N-(4-((2-((3-(4-acetyl)piperazin-1-yl)phenyl)amino)pyrimidin-4-yl)oxy)phenyl)-N-(4-fluorophenyl)cyclopropane-1,1-dicarboxamide (compound **13e**): White solid, yield: 23.07%. ¹H NMR (400 MHz, DMSO-*d*₆) δ 10.15 (s, 1H), 10.07 (s, 1H), 9.38 (s, 1H), 8.34 (d, *J* = 5.6 Hz, 1H), 7.70 (d, *J* = 9.0 Hz, 2H), 7.64 (dd, *J* = 9.1, 5.1 Hz, 2H), 7.20–7.13 (m, 5H), 7.08 (d, *J* = 8.1 Hz, 1H), 6.97 (t, *J* = 8.1 Hz, 1H), 6.47 (dd, *J* = 8.1, 1.7 Hz, 1H), 6.39 (d, *J* = 5.6 Hz, 1H), 3.56–3.47 (dd, *J* = 10.5, 7.0 Hz, 4H), 2.98 (t, *J* = 4.7 Hz, 2H), 2.93 (t, *J* = 4.9 Hz, 2H), 2.03 (s, 3H), 1.47 (s, 4H). ¹³C NMR (101 MHz, DMSO-*d*₆) δ 169.82, 168.71 (d, *J* = 4.3 Hz, 1C), 168.60, 160.30 (d, *J* = 7.60 Hz, 1C), 159.95, 157.56, 151.52, 148.56, 141.30, 136.59, 135.66 (d, *J* = 2.5 Hz, 1C), 129.26, 122.85 (d, *J* = 7.9 Hz, 1C), 122.10, 115.62, 115.40, 111.05, 110.13, 107.05, 98.72, 49.23, 45.87, 31.97, 21.64, 15.85. HRMS: *m/z* C₃₃H₃₂FN₇O₄ [M+H]⁺ 610.2500, Found 610.2576. Purity: > 95% (HPLC).

N-(4-fluorophenyl)-N-(4-((2-((3-(piperidin-3-ylcarbamoyl)phenyl)amino)pyrimidin-4-yl)oxy)phenyl)cyclopropane-1,1-dicarboxamide (compound **13f**): White solid, yield: 31.00%. ¹H NMR (500 MHz, DMSO-*d*₆) δ 10.11 (s, 1H), 10.07 (s, 1H), 8.23 (d, *J* = 5.6 Hz, 1H), 8.10 (d, *J* = 8.0 Hz, 1H), 7.67 (d, *J* = 8.9 Hz, 2H), 7.64 (dd, *J* = 8.9, 5.1 Hz, 2H), 7.19–7.12 (m, 4H), 7.07 (t, *J* = 7.8 Hz, 1H), 7.02 (s, 1H), 6.94 (d, *J* = 7.7 Hz, 1H), 6.69 (dd, *J* = 7.9, 1.5 Hz, 1H), 6.07 (d, *J* = 5.4 Hz, 1H), 5.27 (s, 1H), 4.59–4.20 (m, 2H), 3.83–3.74 (m, 1H), 2.88–2.76 (m, 2H), 1.93–1.85 (m, 1H), 1.75–1.68 (m, 1H), 1.64–1.54 (m, 1H), 1.46 (s, 4H), 1.44–1.34 (m, 2H). ¹³C NMR (126 MHz, DMSO-*d*₆) δ 169.81, 168.62 (d, *J* = 11.21 Hz, 1C), 167.20, 161.64, 160.43, 159.70, 157.79, 148.95, 148.31, 136.40, 136.11, 135.63 (d, *J* = 1.61 Hz, 1C), 129.02, 122.88

(d, $J = 7.70$ Hz, 1C), 121.96, 116.86, 115.58, 115.41, 115.05, 113.40, 95.84, 48.53, 46.15, 43.81, 31.91, 30.76, 23.97, 15.91. HRMS: m/z $C_{24}H_{20}FN_7O_3$ $[M+H]^+$ 610.2500, Found 610.2576. Purity: > 95% (HPLC).

N-(4-fluorophenyl)-*N*-(4-((2-((4-(piperidin-3-ylcarbamoyl)phenyl)amino)pyrimidin-4-yl)oxy)phenyl)cyclopropane-1,1-dicarboxamide (**compound 13g**): White solid, yield: 28.15%. 1H NMR (500 MHz, DMSO- d_6) δ 10.10 (s, 1H), 10.08 (s, 1H), 8.22 (d, $J = 5.5$ Hz, 1H), 7.81 (d, $J = 7.9$ Hz, 1H), 7.69–7.61 (m, 4H), 7.58 (d, $J = 8.4$ Hz, 2H), 7.15 (t, $J = 8.2$ Hz, 4H), 6.54 (d, $J = 8.4$ Hz, 2H), 6.06 (d, $J = 4.9$ Hz, 1H), 5.64 (s, 1H), 4.62–4.15 (m, 2H), 3.83–3.72 (m, 1H), 2.82 (t, $J = 11.5$ Hz, 2H), 1.88 (d, $J = 9.6$ Hz, 1H), 1.71 (d, $J = 11.6$ Hz, 1H), 1.61–1.51 (m, 1H), 1.46 (s, 4H), 1.44–1.33 (m, 2H). ^{13}C NMR (126 MHz, DMSO- d_6) δ 169.81, 168.62 (d, $J = 9.89$ Hz, 1C), 166.27, 161.62, 160.39, 159.70, 157.79, 152.00, 148.32, 136.37, 135.62 (d, $J = 1.39$ Hz, 1C), 129.33, 122.88 (d, $J = 7.70$ Hz, 1C), 122.04, 121.94, 115.59, 115.41, 112.95, 95.78, 48.76, 45.99, 43.83, 31.88, 30.93, 24.04, 15.92. HRMS: m/z $C_{24}H_{20}FN_7O_3$ $[M+H]^+$ 610.2500, Found 610.2567. Purity: > 95% (HPLC).

N-(4-fluorophenyl)-*N*-(4-((2-((4-(4-methylpiperazine-1-carbonyl)phenyl)amino)pyrimidin-4-yl)oxy)phenyl)cyclopropane-1,1-dicarboxamide (**compound 13h**): White solid, yield: 18.28%. 1H NMR (400 MHz, DMSO- d_6) δ 10.18 (s, 1H), 10.09 (s, 1H), 9.80 (s, 1H), 8.38 (d, $J = 5.6$ Hz, 1H), 7.71 (d, $J = 9.0$ Hz, 2H), 7.65 (dd, $J = 9.1, 5.1$ Hz, 2H), 7.58 (d, $J = 8.5$ Hz, 2H), 7.21 (d, $J = 9.0$ Hz, 2H), 7.19–7.13 (m, 4H), 6.48 (d, $J = 5.6$ Hz, 1H), 3.46 (s, 4H), 2.32 (s, 4H), 2.21 (s, 3H), 1.50 (s, 4H). ^{13}C NMR (101 MHz, DMSO- d_6) δ 170.11, 169.51, 168.71, 160.41, 159.90, 157.56, 148.52, 141.96, 136.78, 135.62 (d, $J = 2.5$ Hz, 1C), 128.19, 122.89 (d, $J = 7.9$ Hz, 1C), 122.51, 122.33, 118.39, 115.62, 115.40, 99.15, 54.92, 45.97, 31.81, 31.62, 16.07. HRMS: m/z $C_{33}H_{32}FN_7O_4$ $[M+H]^+$ 610.2500, Found 610.2568. Purity: > 95% (HPLC).

N-(4-fluorophenyl)-*N*-(4-((2-((4-(phenylsulfonamido)phenyl)amino)pyrimidin-4-yl)oxy)phenyl)cyclopropane-1,1-dicarboxamide (**compound 13i**): White solid, yield: 21.35%. 1H NMR (500 MHz, DMSO- d_6) δ 10.21 (s, 1H), 10.06 (s, 1H), 9.94 (s, 1H), 9.47 (s, 1H), 8.30 (d, $J = 5.6$ Hz, 1H), 7.70 (t, $J = 9.6$ Hz, 4H), 7.65 (dd, $J = 8.9, 5.1$ Hz, 2H), 7.59 (t, $J = 7.4$ Hz, 1H), 7.53 (t, $J = 7.7$ Hz, 2H), 7.41 (d, $J = 8.3$ Hz, 2H), 7.19–7.13 (m, 4H), 6.85 (d, $J = 8.7$ Hz, 2H), 6.36 (d, $J = 5.6$ Hz, 1H), 1.52 (d, $J = 4.8$ Hz, 4H). ^{13}C NMR (126 MHz, DMSO- d_6) δ 169.99, 168.83, 168.65, 160.28, 160.03, 159.72, 157.81, 148.43, 139.99, 137.55, 136.77, 135.58 (d, $J = 2.49$ Hz, 1C), 133.15, 131.39, 129.57, 127.17, 122.94 (d, $J = 7.88$ Hz, 1C), 122.32, 122.08 (d, $J = 10.53$ Hz, 1C), 119.88, 115.60, 115.43, 98.61, 31.84, 16.02. HRMS: m/z $C_{33}H_{32}FN_7O_4$ $[M+H]^+$ 639.1748, Found 639.1833. Purity: > 95% (HPLC).

N-(4-fluorophenyl)-*N*-(4-((2-((4-(2-(4-methylpiperazin-1-yl)propanamido)phenyl)amino)pyrimidin-4-yl)oxy)phenyl)cyclopropane-1,1-dicarboxamide (**compound 13j**): White solid, yield: 23.75%. 1H NMR (400 MHz, DMSO- d_6) δ 10.20 (s, 1H), 10.13 (s, 1H), 9.59 (s, 1H), 9.53 (s, 1H), 8.38 (d, $J = 5.6$ Hz, 1H), 7.77 (d, $J = 8.9$ Hz, 2H), 7.69 (dd, $J = 9.1, 5.1$ Hz, 2H), 7.53 (d, $J = 8.7$ Hz, 2H), 7.43 (d, $J = 8.9$ Hz, 2H), 7.26–7.18 (m, 4H), 6.42 (d, $J = 5.6$ Hz, 1H), 3.54–3.46 (m, 1H), 3.23 (q, $J = 6.8$ Hz, 1H), 2.61 (s, 4H), 2.47 (s, 4H), 2.26 (s, 3H), 1.56 (d, $J = 10.5$ Hz, 4H), 1.20 (d, $J = 6.8$ Hz, 3H). ^{13}C NMR (101 MHz, DMSO- d_6) δ 171.15, 170.05, 168.71 (d, $J = 4.87$ Hz, 1C), 160.15, 159.94, 157.55, 148.52, 136.74, 136.31, 135.63 (d, $J = 2.57$ Hz, 1C), 133.10, 122.86 (d, $J = 7.87$ Hz, 1C), 122.35, 122.12, 120.20, 119.52, 115.62, 115.40, 98.36, 63.74, 56.50, 55.27, 45.96, 31.89, 16.00, 13.25. HRMS: m/z $C_{35}H_{37}FN_8O_4$ $[M+H]^+$ 653.2922, Found 653.3001. Purity: > 95% (HPLC).

N-(4-fluorophenyl)-*N*-(4-((2-((3-(2-(4-methylpiperazin-1-yl)acetamido)phenyl)amino)pyrimidin-4-yl)oxy)phenyl)cyclopropane-1,1-dicarboxamide (**compound 13k**): White solid, yield: 40.53%. 1H NMR (400 MHz, DMSO- d_6) δ 10.20 (s, 1H), 10.13 (s, 1H), 9.61 (s, 1H), 9.57 (s, 1H), 8.37 (d, $J = 5.6$ Hz, 1H), 7.76 (s, 1H), 7.74 (d, $J = 9.0$ Hz, 2H), 7.70 (dd, $J = 9.1, 5.1$ Hz, 2H), 7.36 (d, $J = 8.1$ Hz, 1H), 7.27–7.17 (m, 5H), 7.09 (t, $J = 8.1$ Hz, 1H), 6.41 (d, $J = 5.6$ Hz, 1H), 3.18 (s, 2H), 2.62 (s, 6H), 2.56 (s, 2H), 2.34 (s, 3H), 1.52 (s, 4H). ^{13}C NMR (101 MHz, DMSO- d_6) δ 170.01, 168.65 (d, $J = 6.48$ Hz, 1C), 168.37, 160.27 (d, $J = 6.39$ Hz, 1C), 159.94, 157.55, 148.48, 140.90, 138.88, 136.71, 135.67 (d, $J = 2.70$ Hz, 1C), 128.95, 122.82 (d, $J = 7.91$ Hz, 1C), 122.31, 122.19, 115.63, 115.41, 113.65, 110.97, 98.72, 61.70, 54.63, 52.31, 45.38, 31.98, 15.87. HRMS: m/z $C_{34}H_{35}FN_8O_4$ $[M+H]^+$ 639.2765, Found 639.2827. Purity: > 95% (HPLC).

N-(4-((2-((4-(2-((diethylamino)ethyl)amino)acetamido)phenyl)amino)pyrimidin-4-yl)oxy)phenyl)-*N*-(4-fluorophenyl)cyclopropane-1,1-dicarboxamide (**compound 13l**): White solid,

yield: 16.50%. ^1H NMR (400 MHz, $\text{DMSO}-d_6$) δ 10.15 (s, 1H), 10.09 (s, 1H), 9.86 (s, 1H), 9.48 (s, 1H), 8.32 (d, $J = 5.6$ Hz, 1H), 7.71 (d, $J = 8.9$ Hz, 2H), 7.65 (dd, $J = 9.0, 5.1$ Hz, 2H), 7.51 (d, $J = 8.7$ Hz, 2H), 7.40 (d, $J = 8.8$ Hz, 2H), 7.20–7.13 (m, 4H), 6.36 (d, $J = 5.6$ Hz, 1H), 3.36 (s, 3H), 2.90 (s, 2H), 2.75 (s, 6H), 1.51 (d, $J = 5.2$ Hz, 4H), 1.06 (t, $J = 7.1$ Hz, 6H). ^{13}C NMR (101 MHz, $\text{DMSO}-d_6$) δ 170.02, 169.51, 168.74 (d, $J = 2.1$ Hz, 1C), 160.17, 159.94, 157.55, 148.51, 136.72, 136.35, 135.64 (d, $J = 2.6$ Hz, 1C), 133.07, 122.86 (d, $J = 7.8$ Hz, 1C), 122.25 (d, $J = 12.7$ Hz, 1C), 120.10, 119.64, 115.62, 115.40, 98.40, 52.32, 51.46, 46.90, 45.95, 31.92, 15.99, 10.73. HRMS: m/z $\text{C}_{35}\text{H}_{39}\text{FN}_8\text{O}_4$ $[\text{M}+\text{H}]^+$ 655.3078, Found 655.3160. Purity: > 95% (HPLC).

N-(4-((2-((4-(2-((dimethylamino)ethyl)amino)acetamido)phenyl)amino)pyrimidin-4-yl)oxy)phenyl)-*N*-(4-fluorophenyl)cyclopropane-1,1-dicarboxamide (**compound 13m**): White solid, yield: 30.11%. ^1H NMR (400 MHz, $\text{DMSO}-d_6$) δ 10.16 (s, 1H), 10.12 (s, 1H), 9.91 (s, 1H), 9.48 (s, 1H), 8.32 (s, 1H), 7.71 (s, 2H), 7.65 (s, 2H), 7.49 (s, 2H), 7.42 (s, 2H), 7.18 (s, 4H), 6.36 (s, 1H), 3.32 (s, 3H), 2.71 (s, 2H), 2.55 (s, 2H), 2.32 (s, 6H), 1.51 (s, 4H). ^{13}C NMR (101 MHz, $\text{DMSO}-d_6$) δ 170.03, 169.76, 168.76 (d, $J = 3.0$ Hz, 1C), 160.18, 157.57, 148.54, 136.70, 136.30, 135.61 (d, $J = 2.6$ Hz, 1C), 133.12, 122.89 (d, $J = 7.9$ Hz, 1C), 122.32, 122.19, 120.01, 119.65, 115.62, 115.40, 98.39, 58.06, 52.53, 46.03, 44.87, 31.88, 16.02. HRMS: m/z $\text{C}_{33}\text{H}_{35}\text{FN}_8\text{O}_4$ $[\text{M}+\text{H}]^+$ 627.2765, Found 627.2841. Purity: > 95% (HPLC).

N-(4-fluorophenyl)-*N*-(4-((2-((4-(2-(4-(2-methoxyethyl)piperazin-1-yl)acetamido)phenyl)amino)pyrimidin-4-yl)oxy)phenyl)cyclopropane-1,1-dicarboxamide (**compound 13n**): White solid, yield: 33.25%. ^1H NMR (400 MHz, $\text{DMSO}-d_6$) δ 10.14 (s, 1H), 10.09 (s, 1H), 9.48 (s, 1H), 9.46 (s, 1H), 8.32 (d, $J = 5.6$ Hz, 1H), 7.71 (d, $J = 8.8$ Hz, 2H), 7.64 (dd, $J = 8.9, 5.1$ Hz, 2H), 7.47 (d, $J = 8.6$ Hz, 2H), 7.37 (d, $J = 8.8$ Hz, 2H), 7.16 (q, $J = 8.6$ Hz, 4H), 6.36 (d, $J = 5.6$ Hz, 1H), 3.42 (t, $J = 5.8$ Hz, 2H), 3.22 (s, 3H), 3.04 (s, 2H), 2.50 (s, 2H), 2.47 (s, 8H), 1.51 (d, $J = 8.2$ Hz, 4H). ^{13}C NMR (101 MHz, $\text{DMSO}-d_6$) δ 170.05, 168.72, 168.18, 160.15, 157.56, 148.54, 136.71, 136.39, 135.63 (d, $J = 2.5$ Hz, 1C), 132.92, 122.87 (d, $J = 7.9$ Hz, 1C), 122.35, 122.17, 120.33, 119.54, 115.62, 115.40, 98.36, 70.34, 62.22, 58.46, 57.46, 53.42, 53.27, 31.89, 16.01. HRMS: m/z $\text{C}_{36}\text{H}_{39}\text{FN}_8\text{O}_5$ $[\text{M}+\text{H}]^+$ 683.3027, Found 683.3107. Purity: > 95% (HPLC).

3.1.4. Preparation of *N*-(4-Hydroxyphenyl)-1,5-dimethyl-3-oxo-2-phenyl-2,3-dihydro-1H-pyrazole-4-carboxamide (Intermediate 15)

To a solution of 4-antipyrine acid (**14**, 2.0 g, 8.61 mmol) and 4-aminophenol (**10**, 1.13 g, 10.33 mmol) in DMF (20 mL), HBTU (3.92 g, 10.33 mmol) and TEA (2.61 g, 25.84 mmol) were added. The reaction solution was stirred at room temperature for 8 h and monitored by TLC. The reaction solution was poured into ice water (200 mL), and the precipitate was filtered off, washed, and dried in a vacuum to yield intermediate **15** as a white solid (1.75 g, 63.0%), which can be used to the next step without any purification.

3.1.5. Preparation of *N*-(4-((2-Chloropyrimidin-4-yl)oxy)phenyl)-1,5-dimethyl-3-oxo-2-phenyl-2,3-dihydro-1H-pyrazole-4-carboxamide (Intermediate 16)

To a solution of the intermediate **15** (1.75 g, 5.41 mmol) and 2,4-dichloropyrimidine (0.81 g, 5.41 mmol) in DMF (15 mL), K_2CO_3 (0.82 g, 5.95 mmol) was added. The mixture was stirred at 80 °C for 4.5 h. The reaction solution was poured into ice water (100 mL), and the precipitate was filtered off, washed, and dried in a vacuum to yield intermediate **16** as a white solid (1.85 g, 78.0%), which can be used directly without any further purification.

3.1.6. General Procedure for Preparation of Target Compounds 17a–17h

To a mixture of the intermediate **16** (1.2 mmol), substituted aniline (1.0 mmol) and DMF (8 mL), PTSA (4.00 mmol) was added. The mixture was stirred at 90 °C for 4 h under N_2 atmosphere. The reaction solution was cooled to room temperature, then poured into ice water (100 mL), and the precipitate was filtered off, washed, and dried in a vacuum to obtain the crude product, which was

purified by silica gel chromatography using a mixture of (DCM: MeOH = 100:1–30:1) to afford the product **17a–17h**.

1,5-dimethyl-N-(4-((2-((4-((1-methylpiperidin-4-yl)oxy)phenyl)amino)pyrimidin-4-yl)oxy)phenyl)-3-oxo-2-phenyl-2,3-dihydro-1H-pyrazole-4-carboxamide (compound **17a**): White solid, yield: 15.05%. ¹H NMR (500 MHz, DMSO-*d*₆) δ 10.82 (s, 1H), 9.41 (s, 1H), 8.29 (d, *J* = 5.6 Hz, 1H), 7.68 (d, *J* = 8.8 Hz, 2H), 7.60 (t, *J* = 7.7 Hz, 2H), 7.53 (d, *J* = 7.3 Hz, 1H), 7.45 (d, *J* = 7.5 Hz, 2H), 7.40–7.34 (m, 2H), 7.18 (d, *J* = 8.8 Hz, 2H), 6.71 (d, *J* = 7.7 Hz, 2H), 6.38 (d, *J* = 5.6 Hz, 1H), 4.25 (s, 1H), 3.38 (s, 3H), 2.77 (s, 2H), 2.74 (s, 3H), 2.45 (s, 2H), 2.31 (d, *J* = 13.7 Hz, 3H), 1.90 (s, 2H), 1.68 (s, 2H). ¹³C NMR (126 MHz, DMSO-*d*₆) δ 170.12, 163.52, 161.67, 160.36, 160.15, 154.26, 151.89, 148.17, 136.67, 134.09, 133.49, 129.97, 129.33, 127.59, 123.09, 120.95, 120.76, 116.33, 97.94, 97.60, 44.97, 33.83, 21.25, 11.98. HRMS: *m/z* C₃₄H₃₆N₇O₄ [M+H]⁺ 606.2751, Found 606.2832. Purity: > 95% (HPLC).

N-(4-((2-((3-((2-methoxyethyl)amino)phenyl)amino)pyrimidin-4-yl)oxy)phenyl)-1,5-dimethyl-3-oxo-2-phenyl-2,3-dihydro-1H-pyrazole-4-carboxamide (compound **17b**): White solid, yield: 5.80%. ¹H NMR (500 MHz, DMSO-*d*₆) δ 10.82 (s, 1H), 9.28 (s, 1H), 8.31 (d, *J* = 5.4 Hz, 1H), 7.69 (d, *J* = 8.5 Hz, 2H), 7.60 (t, *J* = 7.4 Hz, 3H), 7.52 (t, *J* = 7.2 Hz, 1H), 7.45 (d, *J* = 7.4 Hz, 2H), 7.19 (d, *J* = 8.6 Hz, 2H), 6.87–6.77 (m, 3H), 6.36 (d, *J* = 5.4 Hz, 1H), 6.16 (d, *J* = 6.8 Hz, 1H), 3.42 (t, *J* = 5.5 Hz, 2H), 3.37 (s, 3H), 3.24 (s, 3H), 3.05 (s, 2H), 2.72 (s, 3H). ¹³C NMR (126 MHz, DMSO-*d*₆) δ 169.92, 163.53, 161.65, 160.35, 160.23, 154.29, 149.19, 148.09, 141.27, 136.65, 133.52, 129.95, 129.32, 129.04, 127.58, 122.77, 120.61, 107.94, 106.65, 103.26, 98.29, 97.57, 70.93, 58.42, 42.94, 33.79, 11.93. HRMS: *m/z* C₃₁H₂₁N₇O₄Na [M+Na]⁺ 588.2438, Found 588.2337. Purity: > 95% (HPLC).

1,5-dimethyl-N-(4-((2-((3-((1-methylpiperidin-4-yl)oxy)phenyl)amino)pyrimidin-4-yl)oxy)phenyl)-3-oxo-2-phenyl-2,3-dihydro-1H-pyrazole-4-carboxamide (compound **17c**): White solid, yield: 7.01%. ¹H NMR (500 MHz, DMSO-*d*₆) δ 10.81 (s, 1H), 9.51 (s, 1H), 8.35 (d, *J* = 5.5 Hz, 1H), 7.68 (d, *J* = 8.7 Hz, 2H), 7.60 (t, *J* = 7.5 Hz, 2H), 7.52 (t, *J* = 7.4 Hz, 1H), 7.45 (d, *J* = 7.5 Hz, 2H), 7.27 (s, 1H), 7.20 (d, *J* = 8.7 Hz, 2H), 7.16 (d, *J* = 7.8 Hz, 1H), 7.00 (t, *J* = 8.0 Hz, 1H), 6.51 (d, *J* = 7.7 Hz, 1H), 6.42 (d, *J* = 5.5 Hz, 1H), 4.30 (s, 1H), 3.34 (s, 2H), 2.93 (s, 2H), 2.72 (s, 3H), 2.45 (s, 3H), 2.00 (s, 2H), 1.76 (s, 2H). ¹³C NMR (126 MHz, DMSO-*d*₆) δ 169.95, 163.51, 161.64, 160.33, 160.13, 157.35, 154.28, 147.98, 141.90, 136.69, 133.50, 129.96, 129.49, 129.33, 127.59, 122.70, 120.68, 112.14, 108.92, 107.25, 98.85, 97.57, 51.75, 44.37, 33.80, 31.62, 30.30, 11.94. HRMS: *m/z* C₃₄H₃₆N₇O₄ [M+H]⁺ 606.2751, Found 606.2823. Purity: > 95% (HPLC).

1,5-dimethyl-N-(4-((2-((4-(4-methylpiperazine-1-carbonyl)phenyl)amino)pyrimidin-4-yl)oxy)phenyl)-3-oxo-2-phenyl-2,3-dihydro-1H-pyrazole-4-carboxamide (compound **17d**): White solid, yield: 63.0%. ¹H NMR (500 MHz, DMSO-*d*₆) δ 10.85 (s, 1H), 9.82 (s, 1H), 8.38 (d, *J* = 5.6 Hz, 1H), 7.71 (d, *J* = 8.8 Hz, 2H), 7.60 (t, *J* = 7.6 Hz, 2H), 7.49–7.56 (m, 3H), 7.45 (d, *J* = 7.3 Hz, 2H), 7.21 (d, *J* = 8.8 Hz, 2H), 7.13 (d, *J* = 8.3 Hz, 2H), 6.51 (d, *J* = 5.6 Hz, 1H), 3.37 (s, 4H), 3.33 (s, 3H), 2.73 (s, 3H), 2.27 (s, 4H), 2.15 (s, 3H). ¹³C NMR (126 MHz, DMSO-*d*₆) δ 170.17, 169.40, 163.51, 161.67, 160.46, 159.84, 154.35, 148.05, 141.99, 136.85, 133.49, 129.95, 129.30, 128.45, 128.17, 127.57, 123.12, 120.68, 118.37, 99.11, 97.65, 54.90, 33.80, 11.98. HRMS: *m/z* C₃₄H₃₄N₈O₄Na [M+Na]⁺ 641.2703, Found 641.2603. Purity: > 95% (HPLC).

N-(4-((2-((4-(4-acetylpiperazin-1-yl)phenyl)amino)pyrimidin-4-yl)oxy)phenyl)-1,5-dimethyl-3-oxo-2-phenyl-2,3-dihydro-1H-pyrazole-4-carboxamide (compound **17e**): White solid, yield: 15.79%. ¹H NMR (500 MHz, DMSO-*d*₆) δ 10.85 (s, 1H), 9.36 (s, 1H), 8.28 (d, *J* = 5.5 Hz, 1H), 7.69 (d, *J* = 8.7 Hz, 2H), 7.60 (t, *J* = 7.6 Hz, 2H), 7.52 (t, *J* = 7.4 Hz, 1H), 7.47 (d, *J* = 7.4 Hz, 2H), 7.26 (s, 2H), 7.16 (d, *J* = 8.8 Hz, 2H), 6.68 (d, *J* = 6.9 Hz, 2H), 6.38 (d, *J* = 5.5 Hz, 1H), 3.48 (s, 4H), 3.40 (s, 3H), 2.99 (s, 2H), 2.87 (s, 2H), 2.74 (s, 3H), 2.00 (s, 3H). ¹³C NMR (126 MHz, DMSO-*d*₆) δ 170.26, 168.66, 163.48, 161.69, 160.29, 160.03, 154.04, 148.29, 145.98, 136.72, 133.47, 133.25, 129.97, 129.38, 127.69, 123.28, 120.82, 120.48, 116.55, 97.44, 50.18, 49.24, 45.98, 33.75, 21.60, 11.88. HRMS: *m/z* C₃₄H₃₄N₈O₄Na [M+Na]⁺ 641.2703, Found 641.2607. Purity: > 95% (HPLC).

N-(4-((2-((3-(4-acetylpiperazin-1-yl)phenyl)amino)pyrimidin-4-yl)oxy)phenyl)-1,5-dimethyl-3-oxo-2-phenyl-2,3-dihydro-1H-pyrazole-4-carboxamide (compound **17f**): White solid, yield: 20.0%. ¹H NMR (500 MHz, DMSO-*d*₆) δ 10.82 (s, 1H), 9.40 (s, 1H), 8.34 (d, *J* = 5.5 Hz, 1H), 7.68 (d, *J* = 8.8 Hz, 2H),

7.60 (t, J = 7.6 Hz, 2H), 7.52 (t, J = 7.4 Hz, 1H), 7.45 (d, J = 7.4 Hz, 2H), 7.19 (d, J = 8.5 Hz, 3H), 7.09 (d, J = 7.3 Hz, 1H), 6.96 (t, J = 8.0 Hz, 1H), 6.51 (d, J = 7.5 Hz, 1H), 6.41 (d, J = 5.5 Hz, 1H), 3.51 (t, J = 5.7 Hz, 4H), 3.37 (s, 4H), 2.96 (s, 4H), 2.72 (s, 3H), 2.01 (s, 3H). ¹³C NMR (126 MHz, DMSO-d₆) δ 169.84, 168.70, 163.53, 161.64, 160.33, 160.26, 154.27, 151.57, 148.05, 141.31, 136.61, 133.51, 129.95, 129.32, 129.14, 127.60, 122.59, 120.57, 111.11, 110.15, 107.18, 98.73, 97.56, 49.29, 48.88, 45.86, 33.78, 21.63, 11.92. HRMS: m/z C₃₄H₃₄N₈O₄Na [M+Na]⁺ 641.2703, Found 641.2599. Purity: > 95% (HPLC).

1,5-dimethyl-N-(4-((2-((6-(2-(4-methylpiperazin-1-yl)acetamido)pyridin-3-yl)amino)pyrimidin-4-yl)oxy)phenyl)-3-oxo-2-phenyl-2,3-dihydro-1H-pyrazole-4-carboxamide (compound **17g**): White solid, yield: 18.6%. ¹H NMR (600 MHz, DMSO-d₆) δ 10.81 (s, 1H), 9.72 (s, 1H), 9.67 (s, 1H), 8.49 (s, 1H), 8.35 (d, J = 5.6 Hz, 1H), 7.98 (s, 1H), 7.88 (d, J = 8.6 Hz, 1H), 7.69 (d, J = 8.9 Hz, 2H), 7.60 (t, J = 7.7 Hz, 2H), 7.52 (t, J = 7.5 Hz, 1H), 7.48–7.43 (m, 2H), 7.20 (d, J = 8.9 Hz, 2H), 6.43 (d, J = 5.6 Hz, 1H), 3.37 (s, 5H), 3.11 (s, 2H), 2.72 (s, 3H), 2.52–2.50 (m, 2H), 2.38 (s, 4H), 2.18 (s, 3H). ¹³C NMR (126 MHz, DMSO-d₆) δ 170.10, 168.61, 163.52, 161.66, 161.66, 160.40, 160.08, 154.31, 147.90, 145.69, 139.23, 136.78, 133.75, 133.50, 129.95, 129.32, 128.77, 127.57, 122.68, 120.68, 113.01, 99.15, 97.62, 61.50, 55.13, 52.97, 46.02, 33.78, 11.94. HRMS: m/z C₃₄H₃₆N₁₀O₄Na [M+Na]⁺ 671.2921, Found 671.2823. Purity: > 95% (HPLC).

1,5-dimethyl-N-(4-((2-((4-(2-(4-methylpiperazin-1-yl)propanamido)phenyl)amino)pyrimidin-4-yl)oxy)phenyl)-3-oxo-2-phenyl-2,3-dihydro-1H-pyrazole-4-carboxamide (compound **17h**): White solid, yield: 33.8%. ¹H NMR (600 MHz, DMSO-d₆) δ 10.81 (s, 1H), 9.55 (s, 1H), 9.49 (s, 1H), 8.32 (d, J = 5.6 Hz, 1H), 7.71–7.67 (m, 2H), 7.60 (t, J = 7.7 Hz, 2H), 7.52 (dt, J = 8.3, 1.5 Hz, 1H), 7.51–7.47 (m, 2H), 7.45–7.42 (m, 2H), 7.37 (d, J = 8.6 Hz, 2H), 7.22–7.18 (m, 2H), 6.37 (d, J = 5.6 Hz, 1H), 3.37 (s, 3H), 3.15 (q, J = 6.8 Hz, 1H), 2.72 (s, 3H), 2.52–2.50 (m, 2H), 2.40 (d, J = 71.7 Hz, 6H), 2.13 (s, 3H), 1.13 (d, J = 6.9 Hz, 3H). ¹³C NMR (126 MHz, DMSO-d₆) δ 171.20, 170.01, 163.52, 161.65, 160.31, 160.17, 154.32, 148.03, 136.71, 133.49, 133.13, 129.95, 129.31, 127.53, 122.77, 120.64, 120.16, 119.56, 98.41, 97.65, 63.77, 55.38, 49.39, 46.16, 33.78, 13.29, 11.94. HRMS: m/z C₃₆H₄₀N₈O₄ [M+H]⁺ 662.3125, Found 662.3207. Purity: > 95% (HPLC).

3.2. Mer and c-Met Inhibitory Activity Assay

The in vitro kinase inhibition assays for all compounds against Mer and c-Met were conducted by Shanghai Bioduro Biological Technology Co., Ltd. (China). The detailed procedures are as follows: Prepare 1x buffer: Assay buffer 1X, MgCl₂ 5mM, DTT 1mM. Compound dilution with DMSO. For test compounds, make 100× final concentration solution. Transfer 100 nL compounds to 384-well plate by using the automated liquid handler. The final DMSO% in the assay is 1%. Dilute enzyme stock solutions with 1X assay buffer to concentration of 0.6nM to make a 2X working solution. Add 5μL to the assay plate manually (final 1nM) with multichannel pipette, Spin down at 1000rpm and centrifuge for 30sec and Incubate 15min at 25°C temperatures. Dilute Substrate solutions with 1X assay buffer. Add 5μL mix or buffer to the assay plate manually (ATP final 3.5uM and TK-Sub-Biotin final 0.5uM) with multichannel pipette, Spin down at 1000rpm and centrifuge for 30sec. After 30°C 60 min, add 10μL of Detection solution (TK-antibody-cryptate final 0.25X and streptavidine-XL 665 final 0.3125 uM) to each well of the assay. Mix briefly with Centrifuge, equilibrate for 60 min. Record luminescence on Envision.

3.3. Antiproliferation Assay

The HepG2, MDA-MB-231, and HCT116 cell lines are derived from our own laboratory. The antiproliferative activities were assessed using the CCK-8 assay. Cell viability was measured according to the manufacturer's instructions for the Cell Counting Kit-8 (Meilunbio, Dalian, China). In this assay, 2.5 × 10³ cells per well were seeded into 96-well plates.

After an initial 12-hour incubation, cancer cells were exposed to varying concentrations of compound **17c** for 72 hours. Following this, CCK-8 solution was added to each well and incubated for an additional 2 hours. The absorbance at 450 nm was then recorded using the BioTek Synergy

HTX microplate reader. The experiment was performed in triplicate and repeated three times. IC₅₀ values for compound **17c** were calculated using GraphPad PRISM 9.5.

3.4. *hERG Potassium Currents Assay*

CHO cells, purchased from Cell Bank of Chinese Academy of Sciences (Cat. No.: SCSP-507), were examined using the QPatch system (Sophion) and the automated whole-cell patch clamp method. The detail procedures are as follows: CHO cells stably expressing the transcript of hERG were investigated by the automated whole-cell patch clamp technique, using the QPatch system (Sophion). Cells were grown in 175 cm² flasks in serum-supplemented F12 medium in 37 °C 5% CO₂ incubator. Two days after plating (at 70-80% confluence), culture medium was removed and cells were washed with 7 mL PBS (Phosphate Buffered Saline), then cells were treated with 3 mL Detachin for 2 min at 37 °C, followed by the addition of 7 mL serum-free medium, cells were resuspended in the growth medium at a density of 2-5*10⁶ cells/mL. The cell suspension was then transferred to the QPatch system, where it was centrifuged; the cells were washed and resuspended in extracellular solution (in mM): 140 NaCl, 5 KCl, 1 CaCl₂, 1.25 MgCl₂, 10 HEPES and 10 Glucose, pH 7.4 with NaOH. The composition of the intracellular solution was (in mM): 140 KCl, 1 MgCl₂, 1 CaCl₂, 10 EGTA and 10 HEPES, pH 7.2 with KOH. The cells were held at -80 mV and activated by a +40 mV pre-pulse of 5 s duration followed by a step to -50 mV for 5 s. The voltage protocol is to be repeated every 15 s, the peak of the tail current evoked by the -50 mV step was recorded and measured as test parameter. The solutions containing the compounds were applied to the cells for 2.5 min following a 5 min baseline recording in extracellular solution. Each cell was received from six escalating concentrations. Each concentration was tested on at least 3 cells (n≥3). The reference compound cisapride was applied at the end of the test compound addition. Data were retrieved and analyzed using Assay Software v5.6.4 provided by Sophion, GraphPad Prism 8 and Excel. The concentrations of compounds to yield 50 % block of the hERG currents (IC₅₀) were obtained by fitting normalized concentration-inhibition relationships to the equation in Prism 8 software.

3.5. *Liver Microsome Stability Assay*

Each test compound was initially dissolved in DMSO to prepare a 10 mM stock solution, which was then diluted to 200 μM using acetonitrile. Incubation mixtures were set up in a total volume of 200 μL, containing 0.1 M PBS (pH 7.4), 2 mM NADPH, 0.2 mg/mL liver microsomes, and 1 μM of the test compound or positive control. After a 5-minute preincubation of all components (except NADPH) at 37 °C, NADPH was added. The mixture was pipette-mixed thoroughly, and 20 μL was immediately transferred to a “Quenching” plate as a 0-minute sample, followed by pipette-mixing. At subsequent time points (5, 15, 30, and 60 minutes), 20 μL aliquots were transferred from the incubate to the “Quenching” plate after pipette-mixing. To each well of the plate, 200 μL of acetonitrile containing the internal standard was added. The plate was then centrifuged at 4000 rpm for 10 minutes. Finally, 50 μL of the supernatant was mixed with 50 μL of deionized water and analyzed by LC-MS/MS.

3.6. *Docking Study*

Molecular docking simulations were performed in our lab. The binding interactions of the compounds were investigated with the aid of Discovery Studio 2019. For this analysis, the X-ray crystallographic structures of MerTK (PDB: 4M3Q) and c-Met (PDB: 3LQ8), both resolved at 1.84 Å resolution, were utilized. The protein-ligand interactions were visualized and analyzed through the interaction mode diagram generated by Discovery Studio 2019.

3.7. *Western Blot Assay*

Western blot assay was performed according to established protocols. HCT colon cancer cells were exposed to the specified concentration of compound **17c** for 24 h, after which whole cell lysate

were prepared using RAPI cell lysis buffer (Beyotime Institute of Biotechnology, China). Primary antibodies, purchased from Beyotime Institute of Biotechnology, were diluted at a ratio of 1:2000. The protein band on polyvinylidene fluoride membranes were visualized and analyzed using Glyco Band-Scan Software Version 4.50. The antibody details are as follows:

Name: Phospho-MER/TYRO3 (Tyr753/Tyr685) antibody, Species: Rabbit, Sequence: synthesized peptide derived from human MER/TYRO3 around the Phosphorylation site of Tyr753/Tyr685, Dilution: 1:2000, RRID number: AB_2840500, Catalogue number: AF8443, Supplier: Affinity Biosciences.

Name: Phospho-c-Met (Tyr1234) antibody, Species: Rabbit, Sequence: synthesized peptide derived from human c-Met around the Phosphorylation site of Tyr1234, Dilution: 1:2000, RRID number: AB_2834564, Catalogue number: AF3129, Supplier: Affinity Biosciences.

3.8. Apoptosis Study

Apoptosis was analyzed in a dose-dependent manner using the One Step TUNEL Apoptosis Assay Kit (Meilunbio, Dalian, China). HCT116 cells (1.5×10^4 cells/well) were seeded onto TC-treated glass coverslips in 24-well plates and incubated for 24 hours. Following this, the cells were exposed to varying concentrations of compound **17c** for 48 hours. After treatment, the cells were fixed with 4% paraformaldehyde and permeabilized with 0.3% Triton-X-100. TUNEL staining was performed as per the manufacturer's guidelines, with DAPI used for nuclear counterstaining. Fluorescent images were obtained using an Olympus microscope. The ED₅₀ value for compound **17c** was calculated using GraphPad PRISM 9.5. Each assay was performed in triplicate and repeated three times for consistency.

3.9. Transwell Assay

Migration assays were conducted using Transwell® inserts (Costar, Cambridge, MA) with an 8 µm pore size polycarbonate membrane. HCT116 cells (1.5×10^5) were seeded into the upper chamber with serum-free medium containing 0.2% BSA, while the lower chamber contained medium supplemented with 15% FBS. Compound **17c** was applied at the specified concentrations to both sides of the membrane. After 24 hours of incubation at 37 °C, the cells were fixed in methanol and stained with 0.1% crystal violet. Non-migrated cells on the upper surface of the membrane were removed using a cotton swab. Five random fields per well were imaged under brightfield microscopy, and the number of migrated cells was quantified using ImageJ software. Each experiment was performed in triplicate.

3.10. Plasma Protein Binding in Plasma

Stock solution (20 mM) of compound **17c** was prepared in DMSO. The stock solution was then diluted into 100 µM with acetonitrile. The HT Dialysis apparatus was assembled according to the manufacturer's instructions. 150 µL of the plasma spiked with 1 µM final compound concentrations was added to one site of well and 150 µL of PBS was added to the opposite side of well (n=3). The plate was equilibrated for 6 hours at 37 °C in a 5% CO₂ incubator. For T0 samples: 200 µL of spiked plasma was stored at -20 °C. For T6 samples: 200 µL of spiked plasma was incubated at 37 °C in a 5% CO₂ incubator for 6 hours. After incubation, 50 µL of the samples (plasma or PBS) was collected into a vessel containing 50 µL of the opposite matrix. 300 µL of acetonitrile with IS were added into the vessels. The 96-well plate was centrifuged at 4000 rpm for 10 min. 50 µL of supernatant was mixed with 50 µL of ddH₂O and then injected onto the LC-MS/MS system for analysis.

3.11. Pharmacokinetic Properties

Male and female SD rats (SLRC Laboratory Animal Inc., Shanghai, China) were used for the study. In the oral (PO) administration, 3 rats per group were given a single 10 mg/kg dose. Blood samples (100 µL per time point) were collected via jugular vein cannula and taken at 5, 15, and 30

minutes, and 1, 2, 4, 8, and 24 h post-dose. For the intravenous (IV) administration, 3 rats per group received 2.0 mg/kg, and blood samples were collected at 5, 15, and 30 minutes, and 1, 2, and 4 hours after dosing. Rats were fasted overnight prior to dosing and remained fasted for 6 h post-dose. Plasma was separated by centrifugation and stored at -40°C until analysis. Compound concentrations were determined by LC/MS/MS (Shimadzu LC-30AD), and pharmacokinetic parameters, including C_{max} , T_{max} , $T_{1/2}$, and $\text{AUC}_{0-\text{inf}}$, were calculated.

4. Conclusions

We report a novel series of dual Mer/c-Met inhibitors, with **17c** emerging as the lead candidate. Molecular docking revealed that **17c** forms hydrogen bonds with Mer (Leu593/Lys619) and c-Met (Met1160/Lys1110/Phe1223), complemented by π - π interaction. **17c** exhibited potent enzymatic inhibition and superior antiproliferative activity over cabozantinib against three cancer cell lines. Pharmacokinetically, **17c** showed 45.3% oral bioavailability (16-fold higher than **18c**), extended half-life (3.46 h), and low hepatic clearance (0.026 mL/min/mg). Safety profiling indicated minimal hERG inhibition. Mechanistically, **17c** induced apoptosis and suppressed HCT116 migration. These data position **17c** as a promising dual Mer/c-Met inhibitor warranting further development.

Supplementary Materials: The following supporting information can be downloaded at the website of this paper posted on Preprints.org, Figure S1: title; Table S1: title; Video S1: title.

Author Contributions: Conceptualization, Investigation, Project administration, Writing—original draft, and Writing—review & editing, J.X.; Investigation, Methodology, Project administration, Software, Writing—original draft, and Writing—review & editing, D.W.; Data curation, Investigation, and Methodology, R.J.; Formal analysis, Investigation, and Software, P.X.; Investigation, Methodology, and Validation, R.R.; Data curation, Investigation, Methodology, Project administration, and Writing—review & editing, D.L. All authors have read and agreed to the published version of the manuscript.

Funding: This work was financially funded by Science Research Project of Hebei Education Department (BJK2024144), College Students' Innovation and Entrepreneurship Training Program (202314432007), Special Project for Basic Research Business Expenses of Provincial Universities (JCYJ2023004), Doctoral Research Fund Project (BSZ2022004), and the National Natural Science Foundation of China (No.82003601).

Institutional Review Board Statement: Not applicable.

Informed Consent Statement: Not applicable.

Data Availability Statement: Structures of all compounds, Raw materials of biology, Mer inhibitory results, c-Met inhibitory results, and ^1H -NMR, ^{13}C -NMR, HRMS, and HPLC spectra of all target compounds are listed in Supplementary Materials. All data supporting this study are available from the corresponding authors upon reasonable request.

Acknowledgments: Thank the Instrumental Analysis Center of Hebei University of Science and Technology for providing HRMS and NMR tests.

Conflicts of Interest: The authors declare no conflict of interest.

Sample Availability: Samples of the compounds are available from the authors.

References

1. Wang, X.; Frye, S. Chapter Nineteen—Mer Receptor Tyrosine Kinase: Therapeutic Opportunities in Oncology, Virology, and Cardiovascular Indications. *Annu. Rep. Med. Chem.* **2014**, *49*, 301–314. DOI: 10.1016/B978-0-12-800167-7.00019-5.
2. Graham, D.K.; DeRyckere, D.; Davies, K.D.; Earp, H.S. The TAM family: phosphatidylserine sensing receptor tyrosine kinases gone awry in cancer. *Nat. Rev. Cancer* **2014**, *14*, 769–785. DOI: 10.1038/nrc3847.

3. Yu, S.; Yi, M.; Qin, S.; Wu, K.M. Next generation chimeric antigen receptor T cells: safety strategies to overcome toxicity. *Mol. Cancer*. **2019**, *18*, 125. DOI: 10.1186/s12943-019-1057-4.
4. Smart, S.; Vasileiadi, E.; Wang, X. The Emerging Role of TYRO3 as a Therapeutic Target in Cancer. *Cancers (Basel)* **2018**, *10*, 474. DOI: 10.3390/cancers10120474.
5. Baladi, T.; Abet, V.; Piguel, S. State-of-the-art of small molecule inhibitors of the TAM family: the point of view of the chemist. *Eur. J. Med. Chem.* **2015**, *105*, 220–237. DOI: 10.1016/j.ejmech.2015.10.003.
6. Davra, V.; Kumar, S.; Geng, K.; Calianese, D.; Mehta, D.; Gadiyar, V.; Kasikara, C.; Lahey, K.C.; Chang, Y.J.; Wichroski, M.; Gao, C.; Lorenzo, M.S.D.; Kotenko, S.V.; Bergsbaken, T.; Mishra, P.; Gause, W.C.; Quigley, M.; Spires, T.E.; Birge, R.B. Axl and MerTK Receptors Cooperate to Promote Breast Cancer Progression by Combined Oncogenic Signaling and Evasion of Host Antitumor Immunity. *Cancer Res.* **2021**, *81*, 698–712. DOI: 10.1158/0008-5472.CAN-20-2066.
7. Park, H.J.; Baen, J.Y.; Lee, Y.J.; Choi, Y.H.; Kang, J.L. The TAM-family receptor Mer mediates production of HGF through the RhoA-dependent pathway in response to apoptotic cells. *Mol. Biol. Cell* **2012**, *23*, 3254–3265. DOI: 10.1091/mbc.E12-01-0029.
8. Nguyen, K.Q.; Tsou, W.I.; Kotenko, S.; Birge, R.B. TAM receptors in apoptotic cell clearance, autoimmunity, and cancer. *Autoimmunity* **2013**, *46*, 294–297. DOI: 10.3109/08916934.2013.794515.
9. Sayama, A.; Okado, K.; Yamaguchi, M.; Samata, N.; Imaoka, M.; Kai, K.; Mori, K. The impact of the timing of dosing on the severity of UNC569-induced ultrastructural changes in the mouse retina. *Toxicol. Pathol.* **2020**, *48*(5), 669–676. DOI: 10.1177/0192623320931415.
10. Koda, Y.; Itoh, M.; Tohda, S. Effects of MERTK inhibitors UNC569 and UNC1062 on the growth of acute myeloid Leukaemia cells. *Anticancer Res.* **2018**, *38*(1), 199–204. DOI: 10.21873/anticancer.12208.
11. DeRyckere, D.; Lee-Sherick, A.B.; Huey, M.G.; Hill, A.A.; Tyner, J.W.; Jacobsen, K.M.; Page, L.S.; Kirkpatrick, G.G.; Eryildiz, F.; Montgomery, S.A.; Zhang, W.; Wang, X.D.; Fry, S.V.; Earp, H.S.; Graham, D.K. UNC2025, a MERTK small-molecule inhibitor, is therapeutically effective alone and in combination with methotrexate in leukemia models. *Clin. Cancer Res.* **2017**, *23*(6), 1481–1492. DOI: 10.1158/1078-0432.CCR-16-1330.
12. Yan, D.; Huelse, J.M.; Kireev, D.; Tan, Z.; Chen, L.; Goyal, S.; Wang, X.; Frye, S.V.; Behera, M.; Schneider, F.; Ramalingam, S.S. MERTK activation drives osimertinib resistance in EGFR-mutant non-small cell lung cancer. *J. Clin. Invest.* **2022**, *132*(15). DOI: 10.1172/JCI150517.
13. Zhang, W.; DeRyckere, D.; Hunter, D.; Liu, J.; Stashko, M.A.; Minson, K.A.; Cummings, C.T.; Lee, M.; Glaros, T.G.; Newton, D.L.; Sather, S. UNC2025, a potent and orally bioavailable MER/FLT3 dual inhibitor. *J. Med. Chem.* **2014**, *57*(16), 7031–7041. DOI: 10.1021/jm500749d.
14. Lee-Sherick, A.B.; Jacobsen, K.M.; Henry, C.J.; Huey, M.G.; Parker, R.E.; Page, L.S.; Hill, A.A.; Wang, X.; Frye, S.V.; Earp, H.S.; Jordan, C.T.; Deryckere, D.; Hraham, D.K. MERTK inhibition alters the PD-1 axis and promotes anti-leukemia immunity. *JCI insight* **2018**, *3*(21). DOI: 10.1172/jci.insight.97941.
15. Zhang, W.; Zhang, D.; Stashko, M.A.; DeRyckere, D.; Hunter, D.; Kireev, D.; Miley, M.J.; Cummings, C.; Lee, M.; Norris-Drouin, J.; Stewart, W.M. Pseudo-cyclization through intramolecular hydrogen bond enables discovery of pyridine substituted pyrimidines as new Mer kinase inhibitors. *J. Med. Chem.* **2013**, *56*(23), 9683–9692. DOI: 10.1021/jm401387j.
16. Shi, C.; Li, X.; Wang, X.; Ding, N.; Ping, Y.; Shi, Y.; Mi, L.; Lai, Y.; Song, Y.; Zhu, J. The proto-oncogene Mer tyrosine kinase is a novel therapeutic target in mantle cell lymphoma. *J. Hematol. Oncol.* **2018**, *11*, 1–13. DOI: 10.1186/s13045-018-0584-6.
17. Hu, L.; Wang, X.; Song, Z.; Chen, F.; Wu, B. Leveraging CAR macrophages targeting c-Met for precision immunotherapy in pancreatic cancer: insights from single-cell multi-omics. *Mol. Med.* **2024**, *30*(1), 231. DOI: 10.1186/s10020-024-00996-4.
18. Barbosa-Matos, C.; Borges-Pereira, C.; Libório-Ramos, S.; Fernandes, R.; Oliveira, M.; Mendes-Frias, A.; Silvestre, R.; Osório, N.S.; Bastos, H.N.; Santos, R.F.; Guimarães, S. Deregulated immune cell recruitment orchestrated by c-MET impairs pulmonary inflammation and fibrosis. *Resp. Res.* **2024**, *25*(1), 1–18. DOI: 10.1186/s12931-024-02884-1.

19. Faiella, A.; Riccardi, F.; Carteni, G.; Chiurazzi, M.; Onofrio, L. The emerging role of c-Met in carcinogenesis and clinical implications as a possible therapeutic target. *J. Oncol.* **2022**, 2022(1), 5179182. DOI: 10.1155/2022/5179182.
20. Lee, M.; Jain, P.; Wang, F.; Ma, P.C.; Borczuk, A.; Halmos, B. MET alterations and their impact on the future of non-small cell lung cancer (NSCLC) targeted therapies. *Expert Opin. Ther. Tar.* **2021**, 25(4), 249–268. DOI: 10.1080/14728222.2021.1925648.
21. Gou, Q.; Gou, Q.; Gan, X.; Xie, Y. Novel therapeutic strategies for rare mutations in non-small cell lung cancer. *Sci. Rep.* **2024**, 14(1), 10317. DOI: 10.1038/s41598-024-61087-2.
22. Cen, S.Y.; Lin, F.; Li, X.; Hu, Y.; Liu, J.P.; Xue, Z.; Gao, Y.; Sun, Y.P.; Zhu, S.; Dang, Y.; Zhao, Y. Crizotinib and its enantiomer suppress ferroptosis by decreasing PE-O-PUFA content. *Cell Death Discov.* **2024**, 10(1), 360. DOI: 10.1038/s41420-024-02127-8.
23. Elghawy, O.; Barsouk, A.; Xu, J.; Chen, S.; Cohen, R.B.; Sun, L. Real word outcomes of cabozantinib therapy in poorly differentiated thyroid carcinoma. *Eur. Thyroid J.* **2024**, 13(6). DOI: 10.1530/ETJ-24-0225.
24. Patil, J.; Bhattacharya, S.; Saoji, S.D.; Dande, P. Cabozantinib-phospholipid complex for enhanced solubility, bioavailability, and reduced toxicity in liver cancer. *Ther. Deliv.* **2025**, 16(1), 25–41. DOI: 10.1080/20415990.2024.2435240.
25. Miao, K.; Zhang, X.; Wang, H.; Si, X.; Zhang, L. Savolitinib versus crizotinib for treating MET positive non-small cell lung cancer. *Thorac. Cancer* **2023**, 14(13), 1162–1170. DOI: 10.1111/1759-7714.14848.
26. Qi, Y.; Li, J.; Lin, S.; Wu, S.; Chai, K.; Jiang, X.; Qian, J.; Jiang, C. A real-world pharmacovigilance study of FDA adverse event reporting system events for Capmatinib. *Sci. Rep.* **2024**, 14(1), 11388. DOI: 10.1038/s41598-024-62356-w.
27. Dhillon, S. Capmatinib: first approval. *Drugs*, **2020**, 80, 1125–1131. DOI: 10.1007/s40265-020-01347-3.
28. Huang, D.W.; Chen, Y.; Yang, J.X.; Zhao, B.Y.; Wang, S.Y.; Chai, T.T.; Cui, J.; Zhou, X. L.; Shang, Z. H. Design, Synthesis, and Biological Evaluation of 2-Substituted Aniline Pyrimidine Derivatives as Potent Dual Mer/c-Met Inhibitors. *Molecules*, **2024**, 29(2), 475. DOI: 10.3390/molecules29020475.
29. Wei, D.S.; Fan, H.; Zheng, K.; Qin, X.; Yang, L.; Yang, Y.; Duan, Y.; Zhang, Q.; Zeng, C.; Hu, L. Synthesis and anti-tumor activity of [1,4] dioxino [2, 3-f] quinazoline derivatives as dual inhibitors of c-Met and VEGFR-2. *Bioorg. Chem.* **2019**, 88, 102916. DOI: 10.1016/j.bioorg.2019.04.010.
30. Gao, G.R.; Li, M.Y.; Lv, Y.C.; Cao, S.F.; Tong, L.J.; Wei, L.X.; Ding, J.; Xie, H.; Duan, W.H. Design, synthesis and biological evaluation of biphenylurea derivatives as VEGFR-2 kinase inhibitors (II). *Chinese Chem. Lett.* **2016**, 27(2), 200–204. DOI: 10.1158/1078-0432.CCR-08-2280.
31. Park, H.; Jung, H.Y.; Mah, S.; Hong, S. Systematic computational design and identification of low Picomolar inhibitors of Aurora kinase A. *J. chem. Inf. Model.* **2018**, 58(3), 700–709. DOI: 10.1021/acs.jcim.7b00671.
32. Huang, D.W.; Yang, J.X.; Zhang, Q.W.; Wang, G.; Zhang, Z.X.; Zhang, Y.; Li, J.Q. Structure-guided design and development of novel N-phenylpyrimidin-2-amine derivatives as potential c-Met inhibitors. *Eur. J. Med. Chem.* **2021**, 223, 113648. DOI: 10.1016/j.ejmech.2021.113648.
33. Hwang, S.T.; Um, J.Y.; Chinnathambi, A.; Alharbi, S.A.; Narula, A.S.; Namjoshi, O.A.; Blough, B.E.; Ahn, K.S. Evodiamine mitigates cellular growth and promotes apoptosis by targeting the c-Met pathway in prostate cancer cells. *Molecules* **2020**, 25(6), 1320. DOI: 10.3390/molecules25061320.
34. Li, J.; Tan, G.S.; Cai, Y.B.; Liu, R.H.; Xiong, X.L.; Gu, B.H.; He, W.; Liu, B.; Ren, Q.Y.; Wu, J.P.; Chi, B.; Zhao, Y.H.; Xu, Y.R.; Zou, Z.X.; Kang, F.H.; Xu, K.P. A novel Apigenin derivative suppresses renal cell carcinoma via directly inhibiting wild-type and mutant MET. *Biochem. Pharmacol.* **2021**, 190, 114620. DOI: 10.1016/j.bcp.2021.114620.
35. Gu, Y.; Chen, Y.; Wei, L.; Wu, S.; Shen, K.; Liu, C.; Dong, Y.; Zhao, Y.; Zhang, Y.; Zhang, C.; Zheng, W. ABHD5 inhibits YAP-induced c-Met overexpression and colon cancer cell stemness via suppressing YAP methylation. *Nat. Commun.* **2021**, 12(1), 6711. DOI: 10.1038/s41467-021-26967-5.

Disclaimer/Publisher's Note: The statements, opinions and data contained in all publications are solely those of the individual author(s) and contributor(s) and not of MDPI and/or the editor(s). MDPI and/or the editor(s) disclaim responsibility for any injury to people or property resulting from any ideas, methods, instructions or products referred to in the content.